UNCOVERING THE FUNDAMENTAL MECHANISMS LEADING TO NUCLEATION AND GROWTH IN THE SOLUTION PROCESSING OF HYBRID ORGANIC INORGANIC PEROVSKITES

A Thesis

Presented to the Faculty of the Graduate School

of Cornell University

in Partial Fulfillment of the Requirements for the Degree of

Master of Science

by

Blaire Aria Sorenson

August 2017

ABSTRACT

Power conversion efficiencies of hybrid organic-inorganic perovskite (HOIP) solar cells now rival those of traditional silicon-based solar cells. Unlike silicon, HOIPs can be processed directly from solution, leading to low-cost and energy-efficient fabrication. While many studies have shown that the composition of these solutions ultimately affects the cells efficiency, the underlying physics governing the solution processing of the final crystalline product is very poorly understood and under-investigated due to the overwhelming complexity of the system. Despite the importance of understanding this correlation between processing and performance, the many choices of species and the processing recipe cannot be fully explored by either an experimental or a computational trial-and-error approach. We need to understand the key rules that underlie the complexation and nucleation processes to help guide this exploration. To start this process, we have performed accurate *ab initio* Density Functional Theory (DFT) calculations of important moieties in solution and, critically, identified the Mayer Bond Order (MBO) as a metric of complexation effectiveness in solutions containing the building blocks of lead halide salts. We provide clear evidence, through a proof of concept involving the additive THTO, that the high bonding power and Lewis basicity, measured by the MBO, provides a computationally efficient and accurate way to determine solvent performance and screen currently unused experimental solvents for their effectiveness, hence precluding the need for experimental trial-and-error. For the second step in the process, determining the mechanism of complexation that leads to perovskite nucleation, we have studied the effect of the bath solvents and anti-solvents on the complexation of lead salts to the chaperone cation (methylammonium, formamidinium or cesium) in solution. Using quantum mechanically modeled systems, we have found that, for each choice of lead-halide (iodine, bromine, chlorine), paired with one of these three cations, the permittivity of each solvent or anti-solvent has a direct effect on the binding energy between the PbX_3 and cation (M) motifs. This work shows that the solvating strength of the bath solvents hinders the formation of the smallest perovskite building

blocks (PbX_3M), while the use of the anti-solvents does not. Specifically, our *ab initio* calculations showed that the binding energy between the two major building blocks that go to make up the final perovskite crystal structure can be increased using a relatively low dielectric solvent. The goal of solution processing is, first, to dissolve the lead salts, and, second, to allow nucleation to occur in solution. Our work suggests that these two concurrent events can be controlled to maximize the objectives of each event over the course of the solution processing cycle to achieve a high nucleation density and large-grain crystal growth.

BIOGRAPHICAL SKETCH

Blaire A. Sorenson attended Northeastern Illinois University and graduated with a Bachelor of Science in Chemistry and Applied Mathematics. She then received her Master of Engineering and Master of Science at the School of Chemical and Biomolecular Engineering at Cornell University. Upon graduation with an M.S. degree, Blaire will continue as a Ph.D. student at the School of material Science and Engineering under the tutelage of Prof. Paulette Clancy.

For Dr. Paulo Acioli, my undergraduate mentor whose computational assignments I purposely avoided.

ACKNOWLEDGEMENTS

First of all I would like to express my deep felt gratitude to my advisor, Dr. Paulette Clancy, a great advisor and inspiring mentor. This project has been guided by her invaluable advice, an open-minded and positive outlook towards complex problems. This thesis could not have been completed without her encouragement and direction.

I am also grateful to Prof. Tobias Hanrath and Prof. Lara Estroff for their assistance through suggestions during the course of my program. I would also like to thank all memeber of the Clancy group and especially Dr. James Stevenson who introduced me to computational tools and provided valuable training and mentoring throughout this research effort.

I would also like to thank our experimental collaborators, Dr. Lynn Loo at Princeton University and Dr. Joshua Choi at the University of Virginia. And a special thanks to the Institute of Computational Science and Engineering at Cornell and Dr. Steve Thompson for the many stimulating conversations and help with computational resources.

TABLE OF CONTENTS

LIST OF TABLES

LIST OF FIGURES

CHAPTER 1

INTRODUCTION

1.1 Solar Cell Photovoltaics Overview

In the 1950's, the development of silicon electronics paved the way for commercial photovoltaics (PVs). The first silicon solar cell was reported in 1954 with a mere 6% efficiency [1]. The high cost of fabrication and low Power Conversion Efficiency (PCE) made these devices of interest, but only to space applications such as satellites where the cost was unimportant. Many satellites used chemical energy stored in nickel-cadmium or silver-zinc based batteries, which had a limited life, dependent on the battery weight and power requirements. The first satellite to employ the use of solar cells for power was Vanguard I, which was launched on March 17, 1958. [2] In the following decades, theoretical work projected that a higher efficiency was possible for this PV material, sparking interest for further research and development. It wasn't until the energy crisis of the 1970's when the need for alternative resources to fossil fuels started a slowly growing demand [3]. PV and wind were at the top of the list for the most viable contenders. In the 1990's the demand for energy security warranted new strategies and processing methodologies to produce more efficient and lower-cost materials. This interest in the expansion of PV coincides with the deregulation of the electricity markets in the united states [4]. Widespread deployment of commercial PV, however, did not occur for two decades after this. It was not until 2010, when the globally installed PV capacity was approximately 40.0 GW.In 2007, global installed PV capacity was under 10 GW. As of 2017, it is over 350 GW [5].

A "solar cell" is the smallest active building block of a PV device. The architecture of a solar panel consists of modules, a collection of multiple cells made of a suitable semiconductor material that are connected in series and parallel. Arranging several of these modules together in an array forms the solar panel. The crucial mechanism by which these solar panels work is the formation

of a $p-n$ junction. A p-type material creates valence electron deficiencies, referred to as holes, whereas an n-type material contributes free electrons. Together these form the $p-n$ junction. The interface of these materials, there is a separation of charge, which induces an electric field, known as the depletion zone. In a semiconductor, when light strikes the material, and energy is absorbed, an electron is dislodged, creating electron-hole mobility. The electric field causes the electron to move to the n-type material and the hole to flow towards the p-type material. This mechanism is known as photogeneration of charge carriers. The resulting separation of charges across this junction creates a potential difference. Connecting this material to an external circuit, allows the charge to travel producing an electrical current that can do useful work.

Employing $p-n$ junction architectures, a number of other semiconductor materials, such as cadmium-sulphide, gallium arsenide and cadmium telluride, have found their place on the PV technology map. To date, silicon is still the leading PV material of choice with commercial efficiencies of 26.6% [6], and, until recently, silicon was thought to be unrivaled in terms of efficacy for its cost.

Hybrid organic-inorganic perovskites (HOIPs) are the most promising recent addition to the list of high-performing photovoltaic materials [7, 8]. HOIPs have improved more quickly than any other new PV material in the past decade, with efficiencies of over 22% being reported since their discovery as potential candidates in 2009 [9–12]. Given any reasonable future improvement in processing protocol or choice of cations and anions, *etc.*, this class of materials can surely be expected to attain a laboratory-generated efficiency that exceeds that of silicon. Indeed, there has been some investigation of a combination of silicon and HOIP materials in a tandem cell [13, 14]. Realizing their promise for commerical viability, of course, also depends on solving issues related to reliability, reproducibility, cost, and longevity. The well-used Figure 1.2 of validated solar cell performance by NREL shows the most up-to-date efficiencies of all PV technologies currently in the commercial market or under study as viable market options. It is, however, worth noting, that it may well not be the case that the economic viability of a given material depends on the active

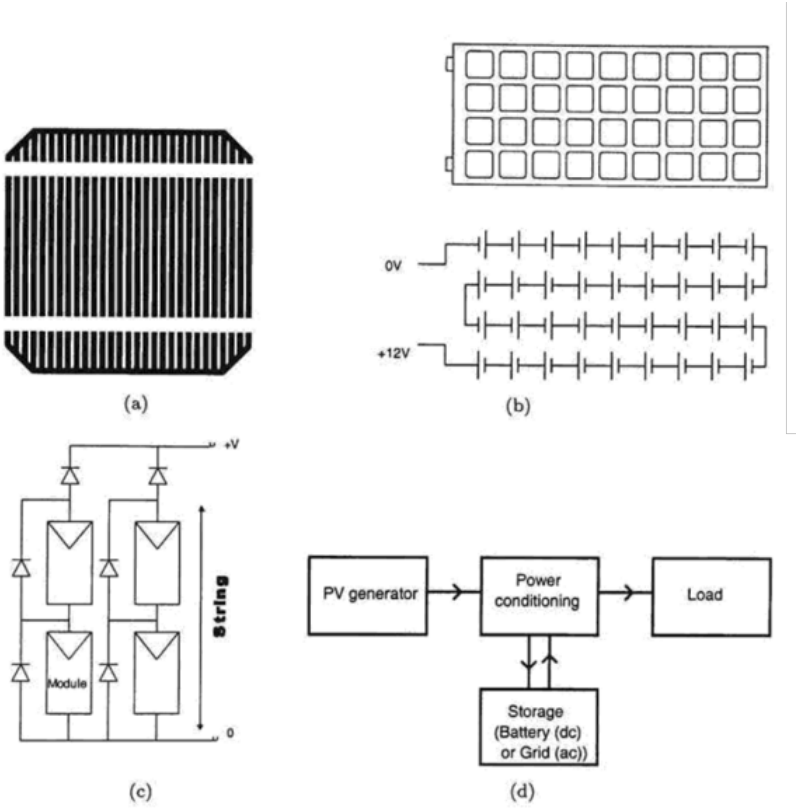

Figure 1.1: (a) Photovoltaic device showing surface contact patterns. (b) a solar cell module. (c) modules connected in an array. (d) photovoltaic integrated with other components for charge regulation and storage.[3]

layer; often, it is the so-called “balance of systems” costs that ultimately determine the economic attractiveness of a given solar cell device.

HOIP perovskite solar cells have shown the most aggressive advancement, in terms of increasing efficiency, in the time since they made their appearance. In order for perovskite-based devices to reach the commercial market, researchers will need to continue to explore the root of the experimentally observed instability and degradation of this material. Despite general recognition of the importance of understanding the correlation between processing, properties and performance, the optimal choice of species that lead ultimately to the final crystalline thin films and the best processing recipe still remains largely determined by an experimental trial-and-error process that cannot possibly explore all possible options for species and processing conditions. In this work, we explore the underlying physics governing the early stages of solution processing of these devices. These stages, involving the solubilization of the lead cation, the complexation of the ancillary cation to the solubilzed lead salt , and the initial nucleation stages, are all poorly understood and under-investigated. The overwhelming complexity afforded by the large set of choices of “building blocks” of the system plays a large role in this, since it precludes a systematic search of the processing space.

1.2 Perovskite Solar Cells

The terminology of a perovskite refers to any material that has the same crystal structure as the mineral calcium titanium oxide, $CaTiO_3$. This is a broad class of materials, including a large number of oxides and of naturally occuring materials. In this thesis, we use the generic term "perovskite" to refer to a sub-set of the class, meaning those which have been explored as potentially active components in photovoltaic devices. These hybrid organic-inorganic perovskite materials (HOIPs) adopt the architecture ABX_3, as seen in Figure 1.3. In this crystal structure, A and B represent cations, where A is typically lead (Pb) or tin (Sn), and B is commonly a methylammonium (MA) or formamadinium (FA) cation or cesium (Cs). X is an anion, here a halide, where X= iodine (I), bromine (Br), or chlorine (Cl). While a number from among the many possible combinations of these materials have been investigated in the laboratory, the most commonly studied ABX_3 combination is currently methylammonium lead iodide, PbI_3MA.

HOIPs are deriving great interest from the semiconductor research community, given their potential to revolutionize the photovoltaics industry. The record for power conversion efficiency of HOIP-based solar cells has reached 22% from under 10% in just a mere six years [15–17], which rivals that of silicon solar cells. HOIP solar cells combine this high efficiency with the advantages offered by solution processability, inexpensive and earth-abundant source materials, light weight, and flexibility, all of which can drastically lower the cost of device fabrication and installation. However, the widespread commercial deployment of HOIP solar cells is currently limited by a poor understanding of the thin film self-assembly processes that is hindering reliable scaling up of the manufacturing process.

Life-cycle analysis has shown that perovskite solar cells have the highest theoretical energy return on energy invested (EROEI) of any PV technology yet known, due to their low-energy solution-processing [18]. It is also becoming clear that the nucleation and crystal growth processes in solution and the quality of the resulting thin-film active layer both play major roles in the effi-

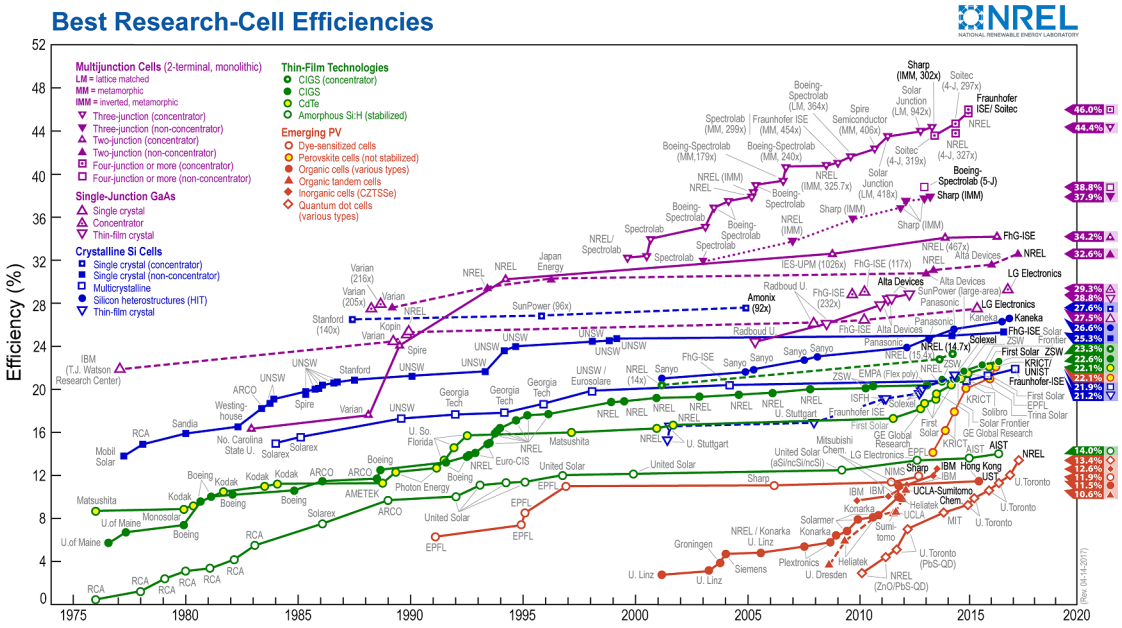

Figure 1.2: Validated PV efficiencies by the National Renewable Energy Laboratory as a function of time and solar cell device type. The performance of HOIP devices (shown as open red circles filled with yellow) begins in 2012 and has increased rapidly to date.[6]

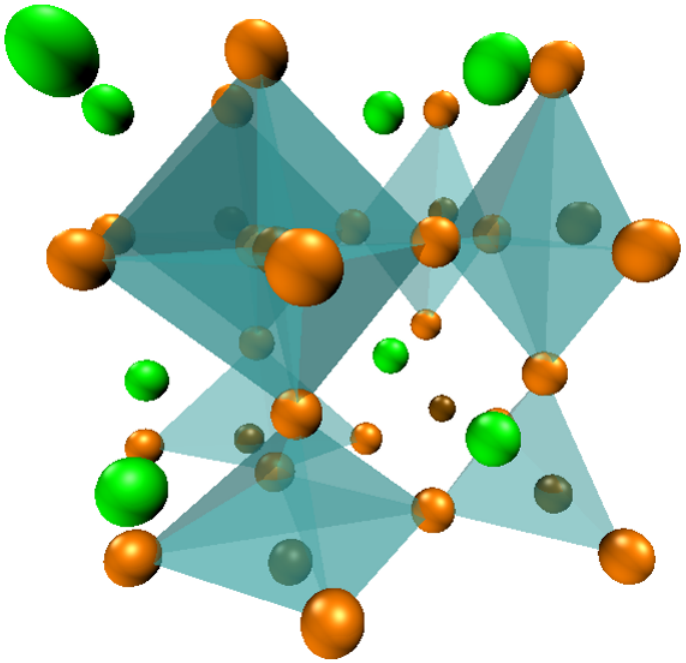

Figure 1.3: Structure of a perovskite unit cell. Orange = halide anion, Brown = A-site cation, Green = B-site cation. Shaded blue areas highlight the octahedral nature of the structure.

ciency and stability of the final product [7, 19, 20]. Despite the progress that has been made, the community's understanding of these HOIP solutions remains limited. It is this lack of understanding is likely to curtail the future growth in the efficiency of new HOIP devices.

1.3 Solution Processing

All of the most effective HOIP synthesis techniques to date have relied on a solution-processing approach [8, 21]. In the so-called"one-step" synthesis process, methylammonium halide CH_3NH_3X is added to a lead halide PbX_2 solution, forming colloidal particles which produce a HOIP film as the solvent is dried, or as an anti-solvent is added [20, 21]. In the "two-step" process, by contrast, the PbX_2 solution is dried into a solid PbX_2 film, in which the formation of an intermediate Pb-DMSO (dimethyl sulfoxide) solid complex has been found to be helpful [8], and to which a CH_3NH_3X solution is added [8]. Other techniques which have been shown to improve performance include solvent evaporation *via* vacuum flashing [22] and post-synthesis solvent annealing using condensing solvent vapor [23–25]. In all of these processes, the quality of the resulting thin films depends intimately on the interaction of the lead halide precursors with the solvents. There are many papers performing calculations on HOIP structures [26–29], but none have focused on HOIP synthesis from solution. The reason for this appears to be that HOIP researchers are most interested in discovering the origins of perovskite efficiency and stability for the bulk films, and in seeking improvements through compositional changes. Less interest has been shown, so far, on changing the processing techniques.

There is an acknowledged demand in the literature for studies that describe the structure of precursor HOIP moieties and how they affect the eventual thin film HOIP product [20, 30]. For example, the drying process which creates the film is controlled by temperature, time, and vapor pressure. The ability to change the solvent mixture could provide researchers the ability to engineer the vapor pressure curve to allow a larger processing "window" and easier, safer man-

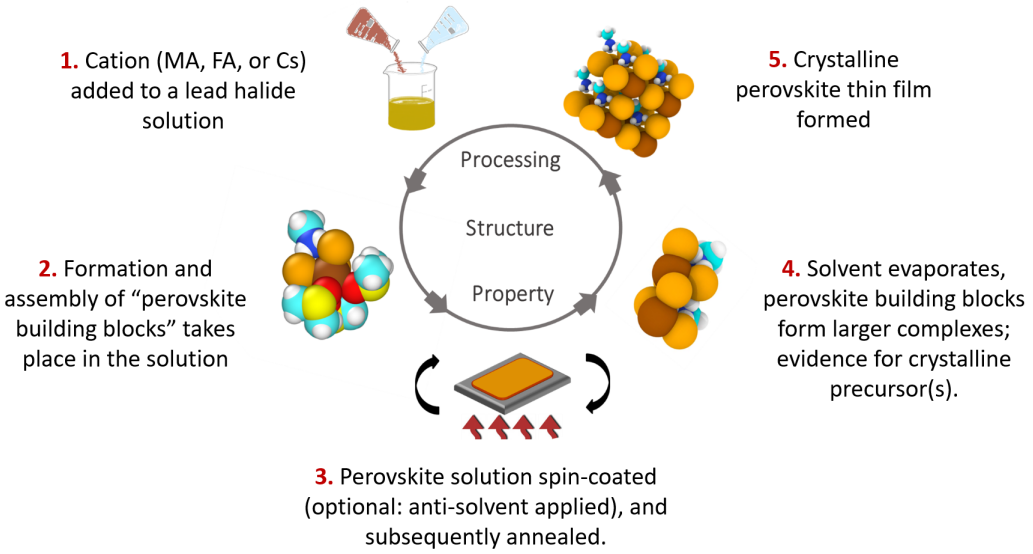

Figure 1.4: Schematic of the HOIP processing cycle showing the five common steps from the initial mixing of the components to the production of a crystalline thin film product.

ufacturing before the final morphology is fixed [31]. Later, as the film deposits, it typically encounters a dewetting problem due to mismatch between the solvent and the TiO_2 or other substrate [32]. Rational "solvent engineering" would allow us to choose a mixture which better matches the substrate while maintaining sufficient PbX_2 solubility. Moreover, it would be useful to understand why some solvents, such as DMSO, form solid solvates with PbX_2, while others do not. The use of solvent blends, such as DMSO and DMF, have produced some of the highest efficiency perovskite solar cells yet known [21]. No information is ever provided in such papers to explain how the solvent blends were chosen. To be able to *rationally* select the optimal solution formulation and thin film processing conditions is acknowledged to be a major step forward, whether the objective is product stability or solar cell efficiency. The first step along the path to such a rational design is the ability to characterize and understand the constituent processes that lead to thin film HOIP formation. This thesis is focused on providing such information.

CHAPTER 2

UNDERSTANDING LEAD COMPLEXATION IN SOLUTION

2.1 Lead-Solvent Coordination

Lead readily forms complexes with halides, known as plumbates. The addition of solvents (of which DMSO and DMF are the most common) provides an electron pair capable of complexing with the lead ion to form a Lewis adduct. As mentioned in a 2016 article by Manser et al. [33] "Proper control over precursor coordination chemistry as a means to improve perovskite solar cell performance should not be underestimated." This article states that: "There are a multitude of different perovskite precursor formulations developed to-date that include mixtures of solvents, halide and molecular ions, and solvated metals. It is important to be cognizant of all the various interactions that can occur between the different components.We still know relatively little about how interactions in solution influence the solid-state product." This chapter is motivated by similar concerns.

Exploring the complexation of lead halide solutions is complicated by determining some characteristic metric (or metrics) that provides the insight we desire. There are many solvent properties which might be able to explain the observed lead ion solubilities and complexation properties of the solvents used in HOIP synthesis. These properties include Hansen solubility parameters, dielectric constant, dipole moment, atomic charges, molecular mass, molecular volume, *etc.* One popular concept currently advanced in the HOIP-related literature is to rank the efficacy of solvents by their relative polarity, $E_N{}^T$ [34], an experimentally determined polarity scale [35]. As we will show, none of these proposed properties are reliable measures of the effectiveness of complexation, including polarity.

Instead, we propose a new predictor. Our hypothesis is that, since the solubility is believed to be dominated by complexation, and complexation is -in turn- dominated by dative bonding, the

solubility should be determined by the solvents electronic state. A simple way as to quantify the electronic state is the Mayer bond order of the solvents most electronegative atom (here, N or O). The Mayer bond order partitions the electron density so as to quantifies the degree of bonding on a scale where a perfectly satisfied double bond is 2.0, a triple bond is 3.0, and so on [36]. The idea that low Mayer bond order correlates with increased ability for dative bonding in passivating molecules has been used previously for polyoxometalates of molybdenum [37]. The concept of reactivity created by low bond order dates back to 1931 and the seminal work of Mulliken [38], who called it "bonding power." Solvents which exhibit a high "bonding power" will also be Lewis bases [34, 39].

To test this hypothesis, we analyzed the complexation behavior of seven solvents: dimethyl sulfoxide (DMSO), dimethyl formamide (DMF), n-methyl pyrrolidone (NMP), gamma-butyrolactone (GBL), acetonitrile (ACN), acetone (ACET), and methacrolein (METH). Five of these (DMSO, DMF, GBL, and ACN) have been used as solvents in previous experimental studies of HOIP materials [21, 40]. We added two more solvents, acetone and methacrolein, although they have not been used experimentally for HOIP synthesis. Their role here was to act as "structural controls," since they have molecular structures similar to DMSO and DMF, respectively, but they differ as explained by Figures 2.1 and 2.2. Dimethylsulfoxide and acetone are analogous in structure and isoelectronic, differing in that DMSO is centered on a hypervalent sulfur atom, while acetone is centered on an octet-satisfying carbon atom. Dimethylformamide and methacrolein differ in structure but not isoelectronic, since methacrolein has an additional double bond which conjugates with its C-O double bond. Comparison of the solution behavior of acetone and methacrolein to their structural analogs, DMSO and DMF, will help us to uncover an all-important connection between structure and properties for the Pb^{2+}/solvent system.

Experiment and *ab initio* calculations agree that Pb (II) is apt to form complexes with polar ligands [41]. Pb (II) complexes with carboxylates are well characterized; in contrast, lead complexes formed in the solutions used in HOIP syntheses have not been characterized at all [41]. A

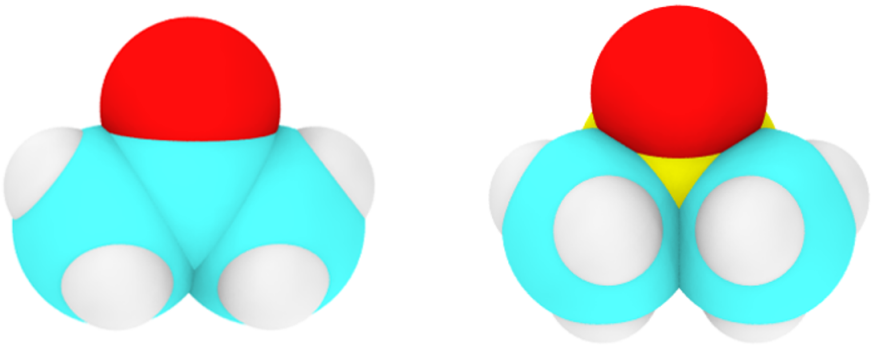

Figure 2.1: Comparison of DMSO (right) and acetone (left). They are analogous in structure and isoelectronic, differing in that DMSO is centered on a hypervalent sulfur atom, while acetone is centered on an octet-satisfying carbon atom. Colors: S=yellow, O=red, C=cyan, H=white

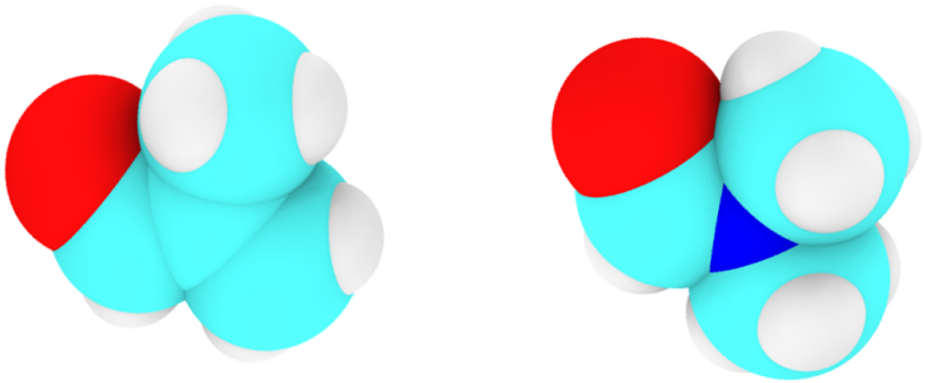

Figure 2.2: Comparison of DMF (right) and methacrolein (left) structures. They are analogous in structure but not isoelectronic, since methacrolein has an additional double bond which conjugates with its C-O double bond. Colors: O = red, N = blue, C = cyan, H = white

key distinction between different types of Pb complexes is whether the distribution of ligands is uniform across the Pb^{2+} surface (holodirected) or not (hemidirected). Valence Shell Electron-Pair Repulsion (VSEPR) theory applied to Pb-O complexes yields the coordination polyhedra shown in Figure 2.3. All known Pb(II) compounds with coordination numbers above 8 are holodirected, while those with coordination numbers of 8 or below may be either holodirected or hemidirected [41]. Yoon *et al.* proposed that Pb^{2+} interacts with solvents at six coordination sites, [30] implying an either holodirected or hemidirected structure. However, we will show below that it is energetically preferred for Pb^{2+} to interact with eight, or even nine, solvent molecules, making it holodirected.

2.2 Computational Experiments of Lead-Solvent Complexation

The solubility of PbX_2 in polar solvents is closely related to the enthalpy of solvation, ΔH_{solv}, defined thermodynamically as the change in enthalpy when a mole of the solute is moved from vacuum to the solvent at infinite dilution. We began by calculating solvated and unsolvated structures for PbX_2, PbX^+, Pb^{2+}, and X^- for three choices of the halide ion, X, as Cl, Br, and I using accurate *ab initio* calculations, described in this section.

We observed that $\Delta H_{solv:Pb^{2+}}$ was quite predictive (representative) of ΔH_{solv} for all Pb-containing solutes. This result implies that the ability to complex with Pb is the primary component of ΔH_{solv} for all PbX_2 salts. The practical advantage of this result is that it allowed us to focus on the behavior of the Pb^{2+} system alone and use our accurate, but computationally expensive, quantum mechanical calculations of $\Delta H_{solv:Pb^{2+}}$ to predict the overall effectiveness of each solvent.

For each solvent, we initialized fifty different sample [Pb^{2+}+ solvent] geometries, and fifty pure solvent cluster geometries, using simulated annealing and *ab initio* optimization, as described below. We chose this large sample size because the complexes have many degrees of freedom and

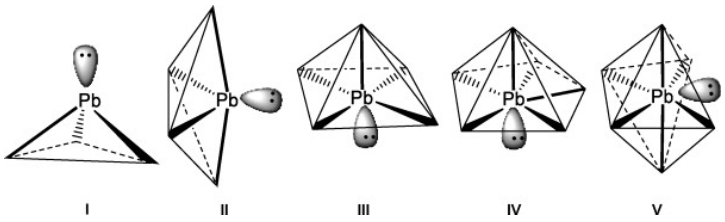

Figure 2.3: Pb^{2+} complex structures suggested by VSEPR theory for different numbers of complexing groups (3-8 from left to right) [41]. Our highly optimized complexes show many more ligands and less order than these regular polyhedra. Figure from Davidovich *et al.*, [41], used with authors' permission

no optimization of a single posited structure will reliably approach the global optimum geometry. We used fifty samples as our initial, very conservative guess, but subsequent testing revealed that sampling twenty geometries is sufficient for almost all our test solvents. Only GBL, with its two oxygen atoms per molecule available as binding sites, showed enough distinct packing states to require more than twenty samples. From the fifty samples, were determined the optimal packing of the solvents on a single Pb_2^+ ion, by conducting an energy comparison across the samples. To determine the lowest energy configuration, we used the additional energy of single optimized solvent molecules to the Pb_2^+- solvent clusters. This allowed us to determine which of the samples was the most energetically favorable by comparing the same number of atoms and stom types in each sample. Once we found the most accurate geometry and lowest energy sample for both the pure solvents and the solutions, we calculated $\Delta H_{solv:Pb^{2+}}$ for each solution as:

$$\Delta H_{solv:Pb^{2+}} = E_{[Pb^{2+}+solvent]} - E_{[solvent]} - E_{[Pb^{2+}]} \tag{2.1}$$

where $E_{[Pb^{2+}+solvent]}$ is the energy of a complex containing Pb^{2+} and solvent cluster, $E_{[solvent]}$ is the energy of a pure solvent cluster, and $E_{[Pb^{2+}]}$ is the energy of an isolated Pb^{2+} ion in vacuum.

We used a "Jacob's Ladder" approach to generate the structures, moving through increasingly accurate (and increasingly computationally expensive) approaches from classical force fields to pure Density Functional Theory (DFT) to more accurate double-hybrid Density Functional Theory [42]. We created initial geometries for the coordination complexes *via* simulated annealing with the semi-empirical OPLS force field. [43] Using those as a starting point, we then optimized the initial geometries using B97-D [44] / def2-TZVP [45] to obtain more accurate structures [46]. Using these optimized geometries, we evaluated the energy and electronic states using the double-hybrid DFT functional PWPB95, [42] with a very large ("quadruple-zeta") basis set, def2-QZVPP(-d,-f) [45]. The use of a quadruple-zeta basis set may not have been necessary, as compared to much less costly triple-zeta basis sets, but we used it in an abundance of caution to avoid the possibility of

basis set superposition error [47] when calculating the energy differences between complexed and uncomplexed states.Each of the *ab initio* calculations required about 200 CPU hours per double-hybrid DFT analysis of each cluster. This expense provides considerable incentive to reduce the amount of samples we used by focusing on the Pb^{2+} solute.

In order to explore the fundamental causes of the solubility differences that we discovered between the solvents, we calculated a series of electronic properties for each solvent, as shown in Table 2.4.4: the dipole moment, Mulliken and Loedwin atomic charges, the occupation of the orbitals for the most electronegative atom, and the unsaturated Mayer bond order for the most polar bond. We calculated these electronic properties using "unrelaxed" electron densities, such that the MP2 correction was not applied to the electronic properties. The unsaturated Mayer bond order appears to be the most useful property. Our results in section 2.4, show the unsaturated Mayer bond order directly correlates to the enthalpy of solvation.

2.3 Physical Laboratory Experiments by Collaborators

2.3.1 Solubility Measurements

Lynn Loo's group at Princeton University performed solubility measurements for lead salts in DMSO, DMF, GBL and acetone. These measurements were made in a nitrogen-filled glove box to avoid water exposure. The solvents and PbX_2 salts were not exposed to air prior to the measurements. This is especially important for DMSO since it is hygroscopic. [31] Pb halide salts with 99.999% purity, and solvents with purities above 99.5%, were purchased from Sigma Aldrich and used without further purification. As a follow-up experiment, they also tested nitromethane solvent with purity of 96% from Acros Organics. No solubility-enhancing additives, such as methylammonium halide, were used in these solutions.

The measurements were taken at room temperature (see Table 2.3.1), approximately 25°C. Each lead salt was added separately to a vial with each solvent and stirred for 15 min. If no precipitate was observed, more salt was added to the solution. The solubility of the lead halide salt was estimated when the precipitate was observed after 30 min of continuous stirring. The expected experimental error is estimated to be less than 3%, based on the difference between two trials for each data point.

	DMSO	DMF	GBL	ACE
PbI_2	600 mg/ml	450 mg/ml	<4 mg/ml	<5 mg/ml
$PbBr_2$	560 mg/ml	350 mg/ml	<4 mg/ml	<4 mg/ml
$PbCl_2$	310 mg/ml	17 mg/ml	<2 mg/ml	<2 mg/ml

Table 2.1: Experimental solubilities of lead halides in pure solvents as measured by the Loo group at Princeton and reported by Stevenson *et al.* [48]

2.3.2 Testing New Additives, THTO, in collaboration with the Choi group at U.Va.

The solvent screening process, described in section 2.4.5, produced many viable candidates for potentially better complexation with lead than the currently used experimental solvents. Joshua Choi's group at the University of Virgina, used a candidate solvent, tetrahydrothiophene-1-oxide (THTO), during solution processing of their thin films. The materials, methylammonium iodide was purchased from Dyesol, PbI_2 (99.999%), $PbCl_2$ (99.999%), tetrahydrothiophene-1-oxide (THTO) (96%), gamma-butyrolactone (GBL) 99%, dimethylformamide (DMF) anhydrous, 99.8%, titanium diisopropoxide bis(acetylacetonate) 75% wt. in isopropanol, isopropanol (IPA) (99%), methanol (99%), nickel acetate tetrahydrate (99%), and diethanolamine (98%) were purchased from Sigma Aldrich and used as received. Dimethylsulfoxide (DMSO) 99.9% was purchased from VWR International. PEDOT:PSS (Clevios HTL solar #1) was purchased from Heraeus and filtered with a 0.45 mm pore size PVDF filter before use. PCBM was purchased from nano-C. ITO substrates (15 ohm cm2) were purchased from Kintec. Aluminum evaporation material (99.999%) was purchased from the Kurt J Lesker company.

A 1-to-1 molar ratio of methylammonium-iodide (MAI) and PbI_2 was dissolved in GBL at 70 C with the THTO additive at a molar ratio of three THTO to one Pb (3 : 1 THTO : Pb). The solution was 30% $MAPbI_3$ by weight. This solution was cooled to room temperature and spin-coated on various substrates such as ITO/PEDOT:PSS, ITO, TiO_2, NiO and SiO_2 at 2000 rpm for 30 seconds. After spin-coating the precursor solution, the samples were annealed at 70 C for 30 minutes to obtain $MAPbI_3$ thin films.

PEDOT:PSS was spin-coated at 1500 rpm for 40 seconds and annealed at 170 C for 4 minutes. For NiOx, a 0.4 mol/L solution of nickel acetate and diethanolamine in methanol was used. This solution was spin-coated at 3000 rpm for 30 seconds and annealed at 400 C for 10 minutes. For TiO_2, titanium diisopropoxide bis(acetylacetonate) in IPA, as purchased from Sigma Aldrich, was

diluted further with IPA until the concentration was 0.3 mol/L. This solution was spin-coated at 3000 rpm for 30 seconds and annealed at 400 C for 10 minutes. Films were spin-coated on a glass/PEDOT substrate at 2000 rpm for 30 seconds from a precursor solution consisting of 0.8 M $PbCl_2$ and 2.4 M MAI in DMF. The films were annealed at 120 C for 10 minutes in ambient conditions (relative humidity = 30%).

A PANalytical X'Pert X-ray diffraction system with a Cu source operating at 40 kV and 40 mA was used to obtain data regarding the structure of the film. All measurements were performed *ex situ* at room temperature. Data were taken at the D-1 beamline at Cornell High Energy Synchrotron Source using X-rays with a wavelength of 0.1168 , a custom precision goniometer, and a Platus 200k two dimensional pixel array detector (Dectris). Samples were spin-coated at the beamline (Chemat), using the same protocol as for the ex-situ XRD measurements. The temperature of the custom-built sample holder was controlled by a temperature controller (Digi-Sense) and the temperature was monitored during X-ray data collection. The X-ray beam was approximately 0.5 mm wide and 0.1 mm high, and illuminated the entire length (5mm) of the sample using an incident angle of typically 0.5. To obtain depth profiles, the incident angle was varied between 0.1 and 0.5 degrees. For all *in situ* data collection, the sample was moved to a new position after three GIXD patterns were collected to avoid beam damage.

2.4 Results and Discussion

2.4.1 Structures of Coordination Complexes

Our calculations of the Pb^{2+} in the presence of a full solvent shell agree with the experimental supposition that the optimum state for Pb^{2+}/solvent clusters is a coordination complex. We found that the preferred Pb^{2+} complex, in the presence of abundant solvent, contains eight or nine solvent molecules forming the first solvation shell around the cation. This is larger than the six molecules

suggested by simple Valence Shell Electron-Pair Repulsion (VSEPR) theory [41] (Figure 2.3) and proposed by Yoon *et al.* [30] This is understandable because VSEPR theory for metal complexes becomes less accurate with increasing atomic number, as might be expected for Pb [30].

Similarities are immediately apparent between the coordination complexes created by the different solvents surrounding a lead cation. The number of electronegative atoms complexed to each Pb^{2+} ion in the DFT-optimized structures is always either 8 or 9 (Figures 2.4 and 2.5) across all the solvents we studied, without regard to their solubility, and regardless even of whether the complexing atom in the solvent is oxygen or nitrogen. This could suggest that the structure is simply the result of packing the electronegative atoms around the positive Pb^{2+} ion. However, the ΔH_{solv} results tell a very different story. Despite their geometric similarities, different solvent complexes produce very different solubilities, as described in the next section.

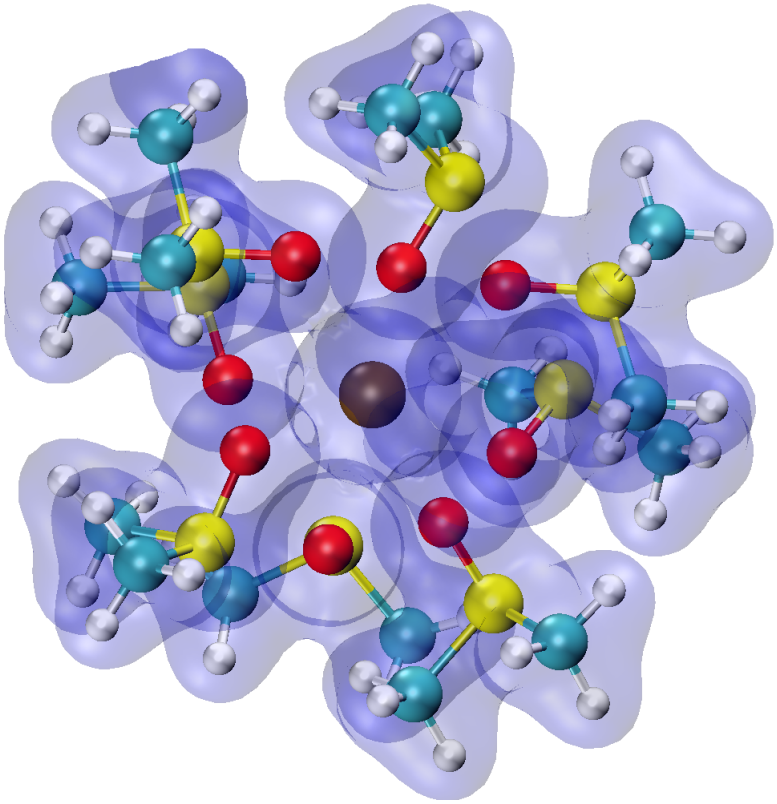

Figure 2.4: Electron density predicted by our *ab initio* calculations surrounding a Pb^{2+}/DMSO cluster with eight coordinated oxygen atoms, the energetically preferred number of neighbors for this solvent. Color key: Pb = brown, S = yellow, O = red, C = cyan, H = white. The blue shading represents the electron density at the 0.005 $e^{-}/Å^{3}$ isosurface.

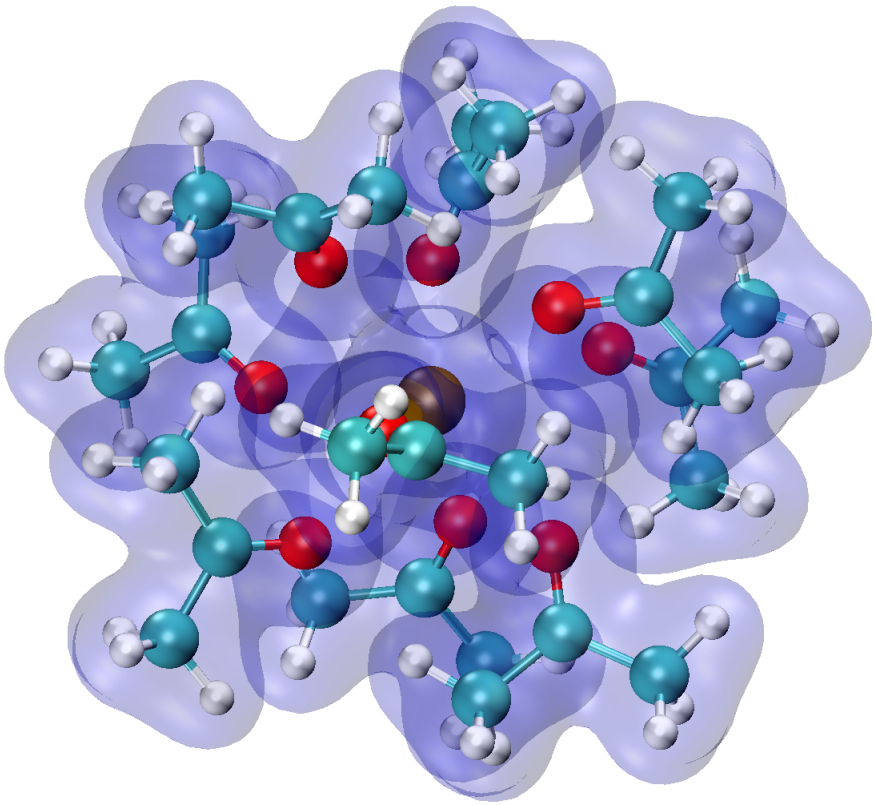

Figure 2.5: Electron density predicted by our *ab initio* calculations surrounding a Pb^{2+}/acetone cluster with nine coordinated oxygen atoms, which we found to be the energetically preferred number of acetone (solvent) neighbors. Color key: Pb = brown, O = red, C = cyan, H = white. The blue shading represents the electron density at the 0.005 $e^{-}/Å^{3}$ isosurface

2.4.2 Computation of ΔH_{solv}

The results of our initial studies on PbX_2, PbX^+, Pb^{2+}, and X^- are shown in Figure 2.6 as a plot of ΔH_{solv} for seven solvents, lead ions, and different halides. In this Figure, the fact that the lines for a given solvent rarely cross each other shows that the relative ranking of $\Delta H_{solv:PbX_n}$ remains consistent, regardless of which PbX_n complex is being used. This motivated our selection, mentioned above, of conducting our subsequent calculations using the Pb^{2+} system alone for our enhanced sampling (*i.e.,* consideration of 50 different initial configurations). The practical advantage of this result is that it allowed us to focus on the Pb^{2+} system alone and conserve our expensive, but accurate, quantum mechanical calculations of $\Delta H_{solv:Pb^{2+}}$ to predict the overall effectiveness of each solvent.

We now turn our attention from considering the solvation of the bare lead cation to the effect of adding counterbalancing halide anions to the system. Figure 2.6 shows that the more halide ions that are attached to the Pb^{2+} ion, the lower the value of ΔH_{solv}. This is consistent with the idea that the halide ions serve to passivate the Pb^{2+}. The contribution of the halides to the solubility follows the expected trend with position in the Periodic Table, with $PbCl_n$ being least soluble and PbI_n being most soluble.

In the same vein, we considered the effect of adding a B-site cation, here, a methylammonium ion (MA), to the Pb halide solutions. The effect is striking, as shown in Figure 2.6. The addition of methylammonium halide stabilizes the PbX_2 complexes by differing extents depending on the choice of halide. A 10 kcal/mol energy stabilization was found for X = Cl, 6.5 kcal/mol for X = Br, and 0.0 for X = I. This result is consistent with the fact that iodine is not known to form strong hydrogen bonds. This computational prediction helps to explain how methylammonium halide acts as such an effective solubility enhancer: its ability to form a complex with up to three halide ions at a time stabilizes agglomerations of Cl^- and Br^-. More fundamentally, the methylammonium triple-halide interaction helps to explain the HOIP synthesis, showing how CH_3NH_3X can act as a

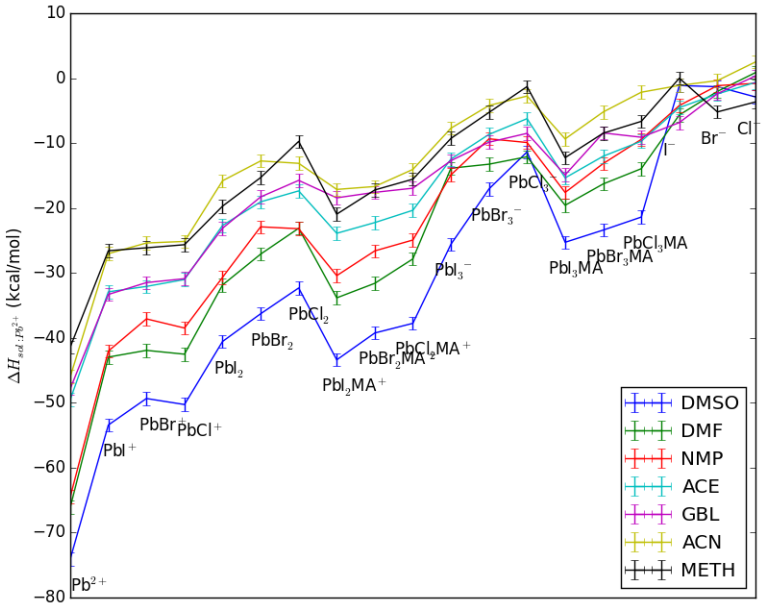

Figure 2.6: *Ab initio* predictions of ΔH_{solv} for PbX_2, PbX^+, Pb^{2+}, and X^- complexes in pure solvents, with $CH_3NH_3^+$ as noted in the labels. Solvent key provided in the inset.

chaperone to bring together the other reactants and form the basis for the perovskite lattice.

2.4.3 Experimental Validation (Loo Group): Solvation

Table 2.3.1 shows the experimental solubilities of Pb salts in the pure solvents found by our Princeton collaborators in the Loo group. A comparison between these solubilities and the values of $\Delta H_{solv:Pb^{2+}}$ is shown in Figure 2.7. Although PbI_2 and $PbBr_2$ show similar solubilities across all studied solvents, $PbCl_2$ demonstrates significantly less solubility in all solvents, with acceptable solubility (in the absence of additives) only in DMSO. In general, for all the systems we studied, DMSO demonstrated the highest solubility, followed by DMF, ACE and GBL. These data show similar trends to the theoretical predictions presented above. The theoretical observations in this study thus help explain the ranking of solvent effectiveness in HOIP processing, since the vast majority of active layers are currently processed using either DMSO or DMF. Moreover, these results help explain the selection of GBL as an additive frequently used for the active layer fabrication, since GBL's low solubility allows it to facilitate aggregation in solution, producing nucleation centers for thin-film formation.

It is interesting to note that the mole ratio of Pb:solvent used in the experimental studies by the Loo group in the DMSO and DMF solutions is large, as high as 1:9 for $PbBr_2$ in DMSO. With solubility enhancers such as methylammonium halide, the mole ratio would be even greater. Interactions between adjacent Pb/solvent complexes will therefore be significant, since each complex prefers to hold 8-9 solvent molecules itself. Infinite dilution, as implied in the definition of enthalpy of solvation, does not hold strictly for such solutions; a soft percolating network of interacting complexes may be a more accurate picture of the system if it becomes necessary to progress to higher-fidelity simulations. Of course, in the absence of an accurate classical force field for the reactions involved, the computational cost of performing such a simulation using *ab initio* calculations would be immense and practically infeasible.

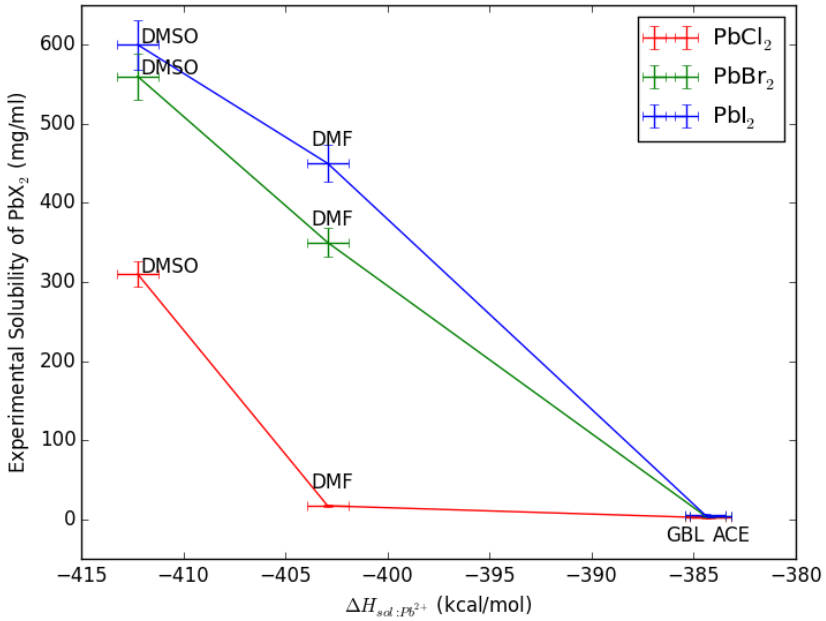

Figure 2.7: Experimental solubility of PbX_2 *vs.* the *ab initio*-derived values of $\Delta H_{solv:Pb^{2+}}$. Note that the energy values are large because the reference state is the vacuum. This relationship shows a linear correlation for the bromide and iodide for DMSO, DMF and GBL (leftmost three points). The result for acetone (the rightmost point) is visually identical to GBL. The correlation for the chloride is flat for much of the range (*i.e.*, for DMF, GBL and acetone) because $PbCl_2$ is a much poorer solute - only DMSO is notably effective. Color key for the halides is given in the inset.

Interestingly, Table 2.3.1 shows that pure acetone provides a similar PbX_2 solubility to that of the much more commonly used GBL. The use of acetone as an additive has not been reported in the literature to the best of our knowledge. It appears that GBL is much more affected than acetone by methylammonium halide solubility enhancers, making GBL practical for HOIP synthesis despite its weak solubility as a pure solvent. Based on our theoretical results, acetone is a plausible supplement to GBL and other solvents in mixtures, especially for solvent mixtures where it is desirable to evaporate one solvent more quickly (such as mixed DMSO/acetone). Further experimental studies will be necessary to test this point, along with theoretical studies to determine why the solubility-enhancing effect of methylammonium appears to vary significantly with respect to the type of solvent.

2.4.4 Fast *ab initio* Prediction of Solubility

The *ab initio* DFT results described above have provided invaluable information, including the structures of the Pb halide complexes with solvents and chaperone ions like methylammonium, and also producing solubility rankings consistent with our experimental results. However, the DFT simulations are quite costly in computational time. Each of these *ab initio* calculations required about 200 hours of CPU time per double-hybrid DFT analysis of each cluster (the most expensive step), totaling 100,000 CPU-hours (10 CPU-years) for all the samples of all the cluster types described in this study. This provides considerable incentive to look for a simpler chemical correlation which is sufficiently predictive to screen good solvents from poor ones for future experiments, without the need to undertake *ab initio* simulations of solvent complexes for eac system under consideration.

We determined that no reliable correlation exists between PbX_2 solubility in a solvent and common solvent properties such as the dielectric constant, molar mass or volume, Hansen solubility parameters, or the relative polarity (see Table 2.2). Each of these properties showed significant discrepancies with our data set. For example, the relative polarity, used to compare DMSO and DMF by Ahn *et al.*, [49] ranks GBL above DMF and acetonitrile above any other solvent, including DMSO [50]. These solvent properties alone are clearly not sufficient to explain the observed differences in the solvents' ability to solvate PbX_2.

Our *ab initio* calculations of the electronic-state properties of each solvent are shown in Table 2.3. These properties include the magnitude of the dipole moment and various attributes of the solvent's most electronegative atom: its Mayer bond order, *p*-orbital occupation, Loedwin atomic charge, and Mulliken atomic charge. We observed a strong, albeit non-linear, correlation between ΔH_{solv} and the Mayer bond order of the solvent's most electronegative atom, which also agrees with the experimental ranking of solubility for PbX_2 (see Figure 2.7).

The Mayer Bond Order is a quantum mechanical estimate of the bond order between two

	Dielectric constant	Molar mass (amu)	Molar volume (cm^3)	Hansen δ_P ($MPa^{1/2}$)[51]	Relative polarity E_T^N [50]
DMSO	46.7	78.1	71.3	16.4	0.444
DMF	36.7	73.1	77.4	13.7	0.386
NMP	32.2	99.1	96.5	12.3	0.355
GBL	40.2	86.1	76.2	16.6[52]	0.420
ACE	20.7	58.1	73.5	10.4	0.355
METH	10.9	70.1	86.7	-	-
ACN	37.5	41.1	52.6	18.0	0.460

Table 2.2: Common macroscopically observable properties of solvents: Dielectric constant, molar mass, molar volume, Hansen solubility parameter and relative polarity. We find that none of these properties are effective at correctly ranking all the solvents considered here in comparison to experiments.

Solvent	Mayer Bond unsaturation	*p*-orbital occupation	Dipole moment (Debye)	Loedwin charge	Mulliken charge
DMSO	0.50	4.73	5.75	-0.32	-0.82
DMF	0.12	4.44	5.37	0.15	-0.51
NMP	0.10	4.44	5.46	0.16	-0.53
GBL	0.01	4.24	6.28	0.21	-0.46
ACE	0.03	4.36	4.09	0.23	-0.47
METH	0.03	4.35	4.04	0.24	-0.41
ACN	-0.03	3.61	5.66	0.04	-0.35

Table 2.3: Electronic properties of solvent molecules: The Mayer bond unsaturation and *p*-orbital occupation of the solvent's electronegative atom are predictive of the experimental ranking of solubility, while the dipole magnitude, Loedwin atomic charge, and Mulliken atomic charge are not.

atoms, inclusive of orbital overlap. It is derived from the electron density using the off-diagonal elements of the Mulliken population matrix PS, where S is the atomic orbital overlap matrix and P is the density matrix. The Mayer bond order includes an accurate contribution from each atom in the bond to the overall bond strength, and is analogous to the electron saturation of the bond between the two atoms [37]. In order to use a common scale for both oxygen and nitrogen, we present the results as "Unsaturated Mayer Bond Order," consisting of the formal bond order minus the calculated Mayer bond order.

$$MBO_{AB} = \sum_{i}^{\text{on A}} \sum_{j}^{\text{on B}} (PS)_{ij}(PS)_{ji} \tag{2.2}$$

$$UMBO_{AB} = FBO_{AB} - MBO_{AB} \tag{2.3}$$

We find that the Mayer bond unsaturation is the best metric to capture the effectiveness of the seven solvents that we studied, unlike other empirical properties such as the Hansen polarity parameter. GBL alone is slightly more effective than its primary oxygen's bond order would suggest, perhaps because GBL contains a second oxygen atom. The use of electronic properties as a screening method is especially useful because the electron density of an arbitrary solvent molecule candidate can be calculated in minutes on a personal computer using free software.

The effectiveness of the Mayer bond order to predict solubility provides further insight that the mechanism of dissolution involves dative bonding rather than simple polarity effects. In a system driven by polarity, the dielectric constant and dipole moment would be effective predictors of solubility [53]. Instead, these properties are not predictive for the Pb^{2+}/solvent system. In contrast, the electronic state of the dative bonding atom (whether oxygen or nitrogen) in the solvent was found to be highly predictive. This implies that the availability of dative bonds dominates over simple polarity effects.

	$\Delta H_{solv:Pb^{2+}}$ (kcal/mol)	MBO (PWPB95)	MBO (B97-D3)	PbI_2 sol. (mg/mL)
DMSO	-412	1.50	1.61	600
DMF	-403	1.88	1.94	450
NMP	-401	1.90	2.01	-
ACE	-384	1.97	2.11	5
GBL	-384	1.99	2.10	4
METH	-379	1.97	2.08	-
ACN	-374	3.03	3.01	-

Table 2.4: Comparison of $\Delta H_{solv:Pb^{2+}}$, Mayer bond order (MBO) calculated at two different levels of theory, and experimental solubility of PbI_2. All three computed metrics ($\Delta H_{solv:Pb^{2+}}$ and both calculations of the MBO) as well as the Loo group's experiments show the same trend with change of solvent.

Figure 2.7 also shows that, in terms of the solvation of Pb^{2+}, acetone and methacrolein fall well below their structural analogs, DMSO and DMF. Even between solvents which are very similar in geometry, there is a striking difference in Pb^{2+} solubility, the physical basis of which only appears when one considers the electronic properties of the solvent. This may also explain why there are no reports of experimental studies using either of these solvents.

Table 2.4 shows $\Delta H_{solv:Pb^{2+}}$ in comparison to predictions of the Mayer Bond Order at two different levels of theory. The comparison of pure DFT (B97-D3) and the more computationally expensive double-hybrid DFT (PWPB95, unrelaxed densities) shows that, while the MBO values change a little, the ordering of the solvents remains consistent with the rankings found using $\Delta H_{solv:Pb^{2+}}$. The difference in MBO value predicted by the two theory levels typically differs by about 0.1 in value. These results show that the Mayer Bond Order is an effective prediction tool with which to rank solvent quality, both at the expensive PWPB95 level of theory and at the inexpensive B97-D3 level. The optimization of a single solvent molecule such as THTO, to obtain the MBO on the less expensive B97-D3 level takes .41 CPU hours, or approximately 25 minutes , where the hybrid level of theory to obtain the MBO requires one hour of CPU time.

2.4.5 UMBO as a screening tool for solvent effectiveness

Dimethylsulfoxide (DMSO) strongly interacts with the Pb^{2+} ion in solution [34, 54], and this property has been used to influence the crystallization process of $MAPbI_3$ with DMSO acting as a complexing additive [21, 34, 55, 56] or as a solvent [57–60]. However, there is nothing to suggest that DMSO is the best additive or solvent that exists; it is simply the most commonly used, presumably because it has been shown to be effective in the laboratory. The Mayer bond order of the oxygen atom present in solvent molecules has been shown to be predictive of the efficacy of the solvent to stabilize Pb^{2+} ions in the $MAPbI_3$ precursor solution. Using the pure DFT-derived Mayer bond order of the oxygen as a metric, given its success above for common HOIP solvents, we then screened some alternative oxygen-containing solvents for their viability in the HOIP synthesis. Potential solvents that were screened are listed in 2.4.5 along with their UMBO. This provides a prediction of the effectiveness of as-yet experimentally untested solvents. The results are shown in Table 2.5 where the S=O functional group was found to be particularly effective at producing low values of the MBO. Hence, our search for solvents better than DMSO at solubilizing the Pb^{2+} cations focused on solvents exhibiting this chemical feature.

The additive tetrahydrothiophene oxide, THTO and diethyl sulfoxide (chemically similar to THTO and DMSO) are also slightly superior to DMSO in Mayer bond unsaturation and do not have the problem of steric hindrance around the oxygen atom. Diethyl sulfoxide has not yet been tested, but THTO bears out the Mayer bond order hypothesis by being a more powerful solvent than DMSO in the Choi group's HOIP syntheses [61]. We conducted additional computational experiments on this suggested additive using the same computational strategy as described in previous sections to obtain the enthalpy of solvation. The resulting enthalpy of solvation and unsaturated Mayer bond order are reported in Figure 2.8 and shows that THTO does have a significantly higher solvation enthalpy than any other experimentally used solvent to date.

Solvent	Unsaturated Mayer Bond Order (B97-D3 theory level)
Diethyl sulfoxide	0.41
Tetrahydrothiophene oxide	0.39
DMSO	0.39
Methyl phenyl sulfoxide	0.37
Diphenyl sulfoxide	0.33
Diethyl sulfite	0.21
Methylsulfonylmethane	0.18
Tetramethylene sulfane	0.17
Ethylene sulfite	0.15
Nitrous acid	0.12
Nitromethane	0.10
Thiosulfuric acid	0.07
Dimethyl sulfate	0.07
Hydrophosphorous acid	0.05
Sulfuric acid	0.05
Phosphoric acid	-0.05

Table 2.5: Prediction of the unsaturated MBO based on the double-bonded oxygen atom as a measure of dative bonding in solvents containing a S=O motif which have not yet been tested in the laboratory. The UMBO values for THTO (0.39) and DMSO (0.39) are shown for comparison as the highest performing additives/solvents. Note that all the results shown in this table were performed at the relatively inexpensive B97-D3 level of theory (different from the PWPB95 values for UMBO reported above.).

The example of nitromethane demonstrates why solvents cannot simply be sorted by their Mayer bond orders, but by their unsaturated Mayer bond order (see equation 2.2). The Mayer bond order of the oxygen atoms in nitromethane (at the B97-D3 level) is 1.40, apparently very unsaturated (compare to DMSO at 1.61). However, because nitromethane's oxygen atoms have symmetrical resonance structures with single and double bonds, nitromethane's oxygen atoms have formal bond orders of only 1.5. Nitromethane's Mayer bond unsaturation is therefore small. This difference is supported by experiments performed by the Loo group at Princeton, which show PbX_2 to be insoluble in nitromethane.

	Solvent	UMBO	ΔH_{solv} (kcal/mol)
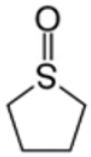	THTO	.52	-538
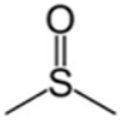	DMSO	.50	-399
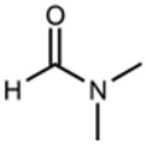	DMF	.12	-393
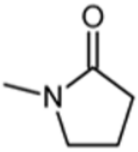	NMP	.10	-392
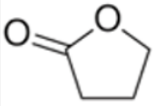	GBL	.01	-377

Figure 2.8: *Ab initio* predictions of ΔH_{solv} for PbX_2, PbX^+, Pb^{2+}, and X^- complexes in pure solvents, with $CH_3NH_3^+$ (MA) as noted in the labels. Solvent key is provided in the inset.

2.4.6 Experimental Validation (Choi group U.Va): Screening

The visual appearance of the $MAPbI_3$ crystallization process with THTO additives offers initial evidence of the reduced (favorable) free energy of the precursor solution. Thin films deposited from a solution of $MAPI_3$ in pure GBL or DMF appear white and hazy after spin-coating, and crystallize into a rough brown film after being heated at 70 C for 3 seconds. These observations are consistent with previous studies [62, 63] that attributed the turbidity to intercalated structure formation [62, 64–66]. In contrast, thin films deposited from solutions of $MAPbI_3$ in DMF or GBL with a molar ratio of 3 THTO molecules to one Pb (3:1 THTO:Pb) have no visible turbidity after spin-coating. These thin films take 30 to 40 seconds at 70 C to turn brown, implying that the presence of THTO significantly delays crystallization of $MAPbI_3$ while suppressing the formation of intermediate structures. By annealing the thin films in a THTO-rich atmosphere, nucleation density can be lowered to the extent that individual brown spots can be seen on the substrate. These spots grow together to form a continuous thin film over the course of 4 to 6 minutes, yielding circular structures up to several millimeters in diameter, as seen in Figure 2.9.

This slow crystallization is in contrast to most other "one step" deposition mechanisms. Many of the previous methods using orthogonal solvent treatment [67, 68], high temperature annealing [19], high pressure gas [63], or flash evaporation of solvent [15] were designed to cause rapid and dense nucleation to obtain pin-hole-free films. Additives have also been used to increase the nucleation density [69], but, to our knowledge, chemical additives have not been previously used to dramatically slow the nucleation as shown in Choi's work.

Addition of THTO in solution formulations was found to result in robustly tetragonally (100)-oriented $MAPbI_3$ thin films. Figure 2.11 shows the XRD patterns obtained from a powder $MAPbI_3$ sample with random crystallographic orientation, tetragonal (110), and tetragonal (100) oriented $MAPbI_3$ thin films. The tetragonal (110)- and (100)- oriented films were obtained from the mixed halide and Choi's THTO methods, respectively. Going beyond 1-dimensional XRD pat-

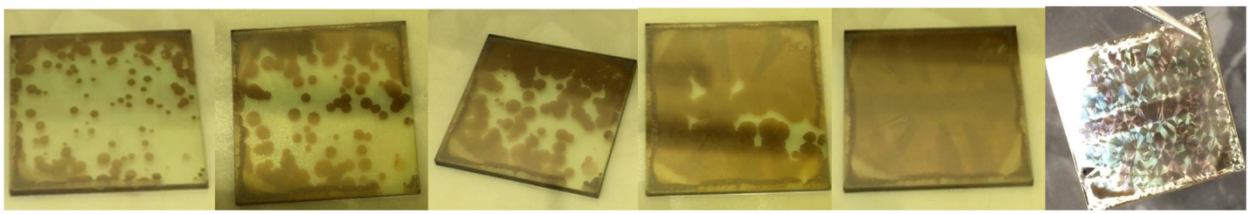

Figure 2.9: $MAPbI_3$ forming from a $MAPbI_3$ precursor solution in a THTO-saturated environment. The brown spots of $MAPbI_3$ grow together to form a film with full coverage. The substrate measures 1 inch by 1 inch.

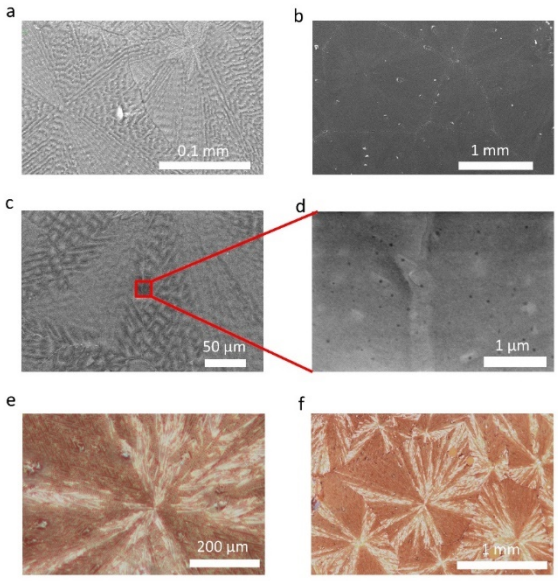

Figure 2.10: (a), (b), (c) SEM images showing the macroscopic $MAPbI_3$ structures on PEDOT produced by the THTO additive method, as well as d) an image of the boundary between these structures taken at higher magnification. (e) and (f) optical images of the $MAPbI_3$ films.

terns, the thin film crystallographic orientation can be unambiguously determined by indexing two-dimensional GIXD patterns with numerous distinctive peaks. The GIXD patterns of tetragonal (110) and tetragonal (100) oriented films are shown in Figure 1 (b) and (c) respectively. The tetragonal (110) orientation is the most commonly observed preferential orientation with $MAPbI_3$ thin films. Several methods [40, 70–73], most notably the mixed halide method [74, 75], have been reported to result in a tetragonal (110) orientation, three methods have yielded tetragonal (100) films [59, 76, 77] and the vast majority of reported methods yield randomly oriented films [8, 20, 67, 78–80]. The tetragonal (100)-oriented $MAPbI_3$ thin films obtained from precursor solutions with THTO additives, as well as the extremely slow crystallization behavior described above, suggest a different crystallization mechanism from any other previously reported methods.

2.5 Summary of Lead-Solvent Complexation

Prior to this work, the only theory of the relative effectiveness of HOIP solvents available in the literature was that they could be sorted by their empirical relative polarities [49] or Hansen solubility parameters [81]. In this work, we have provided clear evidence that the high bonding power and Lewis basicity, as measured by the Mayer bond order, proved more important, in terms of correct predictions, than any other empirical theory or macroscopic and readily available property, such as the relative polarity, Hansen polar parameter, molecular dipole moment, atomic charges, or dielectric constant.

Our *ab initio* DFT studies, in concert with experimental data, show that we can understand the solubility as an energy-driven complexation process, and that the DFT ranking of $\Delta H_{solv:Pb^{2}+}$ correctly matches the experimental ranking of solubility. Furthermore, the Mayer bond order is an effective ranking tool, whether computed at low- or high- levels of theory (*e.g.*, pure DFT or double-hybrid). Importantly, this approach has the advantage that the calculation of the Mayer bond order is *far* less computationally intensive than energy evaluations of the complexes. The

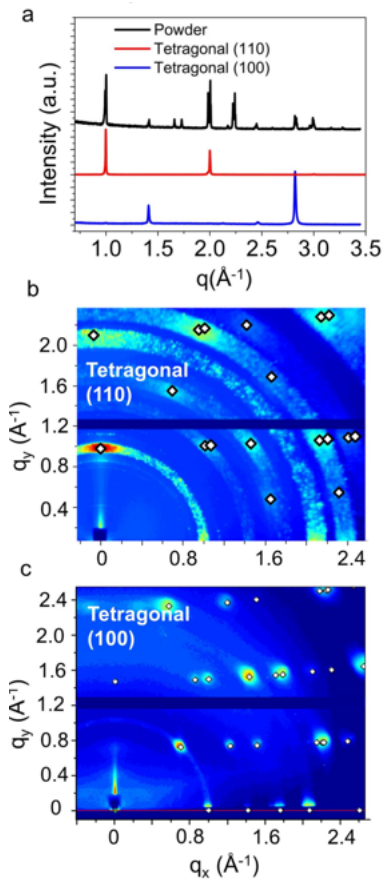

Figure 2.11: (a), (b), (c) SEM images showing the macroscopic $MAPbI_3$ structures on PEDOT produced by the THTO additive method, as well as (d) an image of the boundary between these structures taken at higher magnification. (e) and (f) show optical images of the $MAPbI_3$ films.

computational time needed for a Mayer bond order calculation is approximately 200 times quicker than a typical enthalpy of solvation calculation. And, unlike experimentally-derived solvent properties, it can be readily determined for any conceivable candidate solvent or additive.

Our calculations confirm the experimental observation that the most powerful currently used solvent for HOIP perovskite synthesis is DMSO, followed by DMF. However, we have been able to extend beyond what has been explored in physical laboratories. Using the Mayer bond order as a screening tool for other, as yet untried, solvents, our calculations suggest that nitromethane and THTO have unusually high (and hence promising) unsaturated Mayer bond values. But only THTO has a promising bond *unsaturation* value. This additive was shown by the Choi group at U.Va. to fulfill this promise [61]. The presence of two adjacent oxygen atoms in nitromethane showed the importance of considering the *unsaturated* value of the Mayer bond order, rather than the Mayer bond order itself. Acetone is also surprisingly effective; in the absence of a methylammonium halide solubility enhancer, our calculations predict that it is as effective as GBL. Since acetone is a staple in chemical laboratories, it may be a valuable addition to the HOIP synthesis tool kit, especially with the methylammonium salt and/or in mixtures with other solvents such as DMSO. Use of solvent mixtures has another potential benefit: It offers additional degrees of freedom in the process, allowing a wider variety of desired solubilities, evaporation rates, and colloidal and solid-state complexation behaviors.

The experimentally observed effect of methylammonium halide as a solubility enhancer is addressed by our cluster geometry calculations, which show that the methylammonium ion stabilizes halide solutes. The NH_3^- group can form up to three hydrogen bonds with halide ions, allowing it to stabilize clusters such as PbX_2 and PbX_3. The effect weakens with increasing atomic number of the halide, with PbI_3^+ having little interaction with NH_3^-, reflecting the fact that iodide is less capable of hydrogen-bonding than the other halides. Therefore, while we cannot yet claim that this effect fully explains the enhanced solubility caused by methylammonium halides, at least for the iodide salts, our calculations have uncovered an important role for chaperone cations like MA.

The PbX_2 concentrations observed by our collaborators' experiments are large enough that interactions between adjacent complexes may be significant, especially once methylammonium solubility enhancers are included. High-concentration interactions of this kind might lead to a solution composed of interconnected networks of solvated Pb complexes. Unfortunately, DFT is not computationally efficient enough to simulate such large hypothesized systems, except with supercomputer-class resources. A classical force field, validated against suitably determined DFT results, would be very useful for this purpose. Semi-empirical force fields would be several orders of magnitude faster than DFT. Unfortunately, no adequate reactive force field currently exists for studying HOIP solutions.

We have demonstrated the use of computational screening to rationally select an additive for the $MAPbI_3$ precursor solution that may alter the mechanism and rate of nucleation and growth processes. Specifically, we lowered the free energy of the precursor by incorporating a sulfoxide motif, which strongly interacts with PbI_3MA precursors, allowing an unprecedented degree of control over the nucleation density and growth rate. By altering the relative surface stabilities with chemical additives, our collaborators at U.Va were able to tune the crystallographic orientation of PbI_3MA. The systematic methodology demonstrated in this work will enable more efficient and robust selection of HOIP precursor solution formation, which will lead to more precise degree of control over HOIP thin film formation processes. Ultimately, these advances will contribute to accelerating the progress in HOIP solar cell efficiency improvement, scale-up of device manufacturing, better stability and reliability.

CHAPTER 3

PEROVSKITE BUILDING BLOCKS

3.1 Lead-salt and cation complexation

The use of solvents as a drip treatment during the spin coating process has become one of the most popular means to fabricate high efficiency HOIPs. However, the few reported solvents that have been used experimentally have been selected by a trial-and-error approach. There has yet to be a clear reasoning in the selection of these solvents to promote high-performance perovskite solar cells [82]. For clarification, and following the terminology in the literature, we will refer to the solvents discussed in the previous chapter as "bath solvents," as these are used to solvate the lead salt, and those used in the drip treatment as "anti-solvents." Literature shows, that bath solvents, while successful in dissolving the solid lead salt also have the unwanted tendency to dissolve perovksite precursors as well as the thin film. This is observed in experiments by a color change from black, representative of a perovskite thin film, to yellow, indicating the presence of the perovskite precursor [83]. Anti-solvents assisting in the perovskite film formation include a larger number of solvents that do not dissolve any precursor or the perovskite itself. They are typically non-polar, miscible with the bath solvent, and have lower dielectrics [82]. It is suspected that the working mechanism of an anti-solvent is to speed up the heterogeneous nucleation *via* the creation of an instantaneous local supersaturation on the spinning substrate [67]. The most popular anti-solvents used to date are toluene [8], chlorobenzene [84], and diethyl ether [85]. There have been also recent reports using pyridine [86] and trifluorotoluene [82] as anti-solvents.

In this work, we present a novel approach to redesign the solution processing procedure. We propose that the inclusion of the anti-solvent *prior* to spin coating the perovskite precursor solution will allow for better complexation of the perovskite building blocks that make up the thin film. Traditionally, the anti-solvent is applied after the perovskite precursor solution has been spin-

coated onto the substrate. In doing so, the anti-solvent also acts as a cleansing medium to rid the perovskite precursor film of the unwanted bath solvent. We know the solvation of the lead salt is dominated by the use of polar aprotic solvents (bath solvents), which can be well understood by the unsaturated Mayer bond order of the solvent molecule. We believe the solvating strength of these bath solvents can hinder the formation of perovskite building blocks, as we will discuss in the sections that follow in this chapter. In the presence of anti-solvents, we observe a larger binding energy between the lead salt and the cation compared to that of the bath solvents. We will attribute this difference in binding energy to the permittivity of these individual solvents. Our work suggests that modulating the permittivity of the perovskite processing solution after the solvation of the lead salts should induce the formation of the perovksite building blocks in solution, prior to the spin-coating step. The work described in the following sections further investigates the complexation and binding of the two constituent species that will comprise the final HOIP thin film.

We analyzed the complexation of PbX_3M, where PbX_3 is the lead salt, and M is the organic or inorganic (B-site) cation for all choices of halide and cation, as seen in Figure 3.1. We studied the experimentally used bath solvents in our previous work, including the structural analogues acetone and methacrolein, as well as experimentally used anti-solvents (triflourotoluene, toluene, pyridine and chlorobenzene). In addition, we wanted to expand our search of solvents and anti-solvents, focusing on the relative dielectric constant as a metric as a search criterion for other potential solvents or anti-solvents. A list of all the solvents used in these computational experiments can be seen in Table 3.4. The focus of the computational experiments described in this section was to understand the solvent effect on lead complexation in solution.

3.2 Computational Experiments of PbX_3M complexation in solution

The binding energy of two charged species in solution, as is the case in our study, is closely related to the Coulombic force, which describes the force between two static and charged particles.

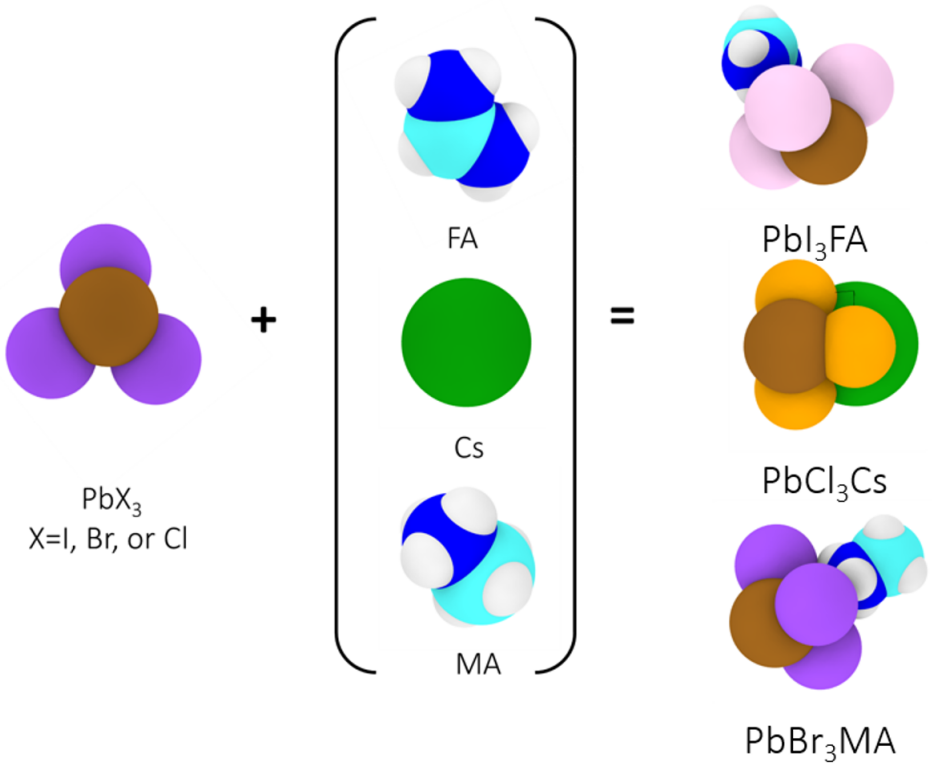

Figure 3.1: Matrix of possible monomer combinations arising from three choices of halide anion and three choices of B-site cation. The right hand side shows just three of the possible monomers which can form from this matrix of options.

Coulomb's law tells us that the force between two charged species is dependent on the permittivity of the medium, the distance between them, and the charge of each species.

$$CoulombicForce = k_e \frac{q_1 q_2}{r^2} \tag{3.1}$$

where k_e, is Coulomb's constant $k_e = 8.99 \times 10^9 Nm^2C^{-2}$ in a vacuum, or $k_e = \frac{1}{4\pi\epsilon_0}$, where ϵ_0 is the permittivity of the medium. q_1 is the charge on species 1, q_2 is the charge on species 2, and r is the distance between the two charged particles.

The binding energy between the two species is defined as the energy needed to be done on the system to pull the two species apart. In our case,

$$E_{Binding} = E_{\mathrm{PbX_3M}} - E_{\mathrm{PbX_3}} - E_M \tag{3.2}$$

where $E_{\mathrm{PbX_3M}}$ is the energy of a single building block containing lead, halide and "M" (the B-site cation), $E_{\mathrm{PbX_3}}$ is the energy of an isolated lead salt, and E_M is the energy of the isolated B-site cation. We began by calculating unsolvated structures for all PbX_3M combinations for three choices of the halide ion, X (Cl, Br, I) and three choices of cations (MA, FA and Cs) using accurate *ab initio* calculations, described below.

For each building block combination, we performed a geometry optimization using the DFT package, Orca [87], the hybrid functional PW6B95 [88] and the polarized basis set TZVPP [89] with dispersion corrections in a vacuum [90, 91]. To reduce the computational effort, the usually highly contracted and chemically inert core basis functions were eliminated by employing Effective Core Potentials (ECPs) [89, 92, 93]. ECP calculations comprise a "valence-only" basis and thus are subject to the "frozen core" approximation. An Effective Core Potential (ECP) was applied to Pb, Cs, I, and Br. The Geometrical Counterpoise Correction (GCP) [94] was employed

to remove artificial over-binding effects from basis set superposition errors (BSSE). The correction uses atomic corrections and thus also yields the ability to correct for intramolecular BSSE. All systems were given a Tight SCF and slow convergence criteria with a grid size of 7. Upon convergence, each system was reoptimized using the same inputs described above, but this time including the SMD option [95, 96]. The SMD solvation model is based on the quantum mechanical charge density of a solute molecule interacting with a continuum description of the solvent. In the model, the full solute electron density is used without defining partial atomic charges. The solvent is not represented explicitly, but rather as a dielectric medium with the surface tension at the solutesolvent boundary. The solvents used in this experiment included bath solvents, previously investigated in Chapter Two, as well as anti-solvents.

3.3 Structures of HOIP Building Blocks

We began by building and optimizing the energy of various orientations of each of the following structures, PbX_3M, PbX_2M and PbXM, for all combinations of halide (X) and B-site cation (M = MA, FA or Cs) in a vacuum. Each sample included a different starting position of the B-site cation relative to the lead salt. Once the samples for all the structures were relaxed, we used the lowest energy conformation from each structural category to further compare and analyze the energetics across all three structural systems for a particular choice of B-site cation. In order to compare these different structures and to determine which conformation was the most stable, we used the additional energy of a single optimized halide ion to the PbXM and PbX_2M. This allows us to determine which of the three structures was the most energetically favorable by comparing the same number of atoms, and atom types in each system. The result of this analysis showed that PbX_3M was the most energetically stable for all the halide and B-site cation combinations compared to PbXM and PbX_2M.

We chose to use this structure, the smallest and most stable building block of the perovskite precursor solution, which we define as a "monomer," a single PbX_3M molecule. Using just this single monomer, nine combinations are possible (three choices of halide and three choices of B-site cation). Studying each of these nine combinations in the 25 pure solvents and anti-solvents that we will discuss in section 3.4, amounts to 225 combinations of building blocks. We are not ignoring the fact that building blocks such as PbX_2M, PbXM or others can exist in solution. Our decision to focus on PbX_3M reduces the vast number of simulations and costly computational time needed to conduct the next step of this investigation, namely, determining the effect of the permittivity of each solvent on the nature of the complexation of the lead salt and cations.

To date, it is unknown to experimentalists and computationalists alike which species are the most important and numerous in the solution. But this information would be extremely beneficial, as it would allow us to tailor the processing recipe to produce a given outcome. To determine which

species has a higher occurrence in the solution would require the ability to perform Molecular Dynamics (MD) simulations of a larger, more representative system. MD simulations would make it possible to observe the presence of all perovskite precursor species, and determine the most likely candidate to form while in solution. As mentioned previously, no suitable force field to conduct these experiments currently exists, which greatly hinders our ability to study large samples of HOIP precursors in solution.

The monomer, as defined above, is composed of a single PbX_3 ion and cation. We analyzed the geometry-optimized structure of each lead salt and cation individually, as well as the monomer complex that they form together. All lead salts of the form PbX_3 assume a trigonal pyramidal structure with a point group of C_{3V}. The point group of a spherical entity, such as cesium, is given the label K, and this is the point group used for free atoms in the gas phase. This is the highest symmetry for a 3D object, having an infinite number of rotation axes of infinite order. Methylammonium also belongs to the point group C_{3V}, and formamadinium to C_{1V}. For the cesium ion, regardless of the starting configuration, all our simulations resulted in the same relaxed position, centered between all three halide atoms on the lead salt. Methylammonium, showed a similar behavior, with all three amine hydrogens in close contact with the halide atoms of the lead salt. These configurations can be seen in Figure 3.2. In the case of formamadinium, the orientation of the cation with respect to the lead salt resulted in the same orientation for the two smaller halides, bromine and chlorine, but a different one for iodine, as seen in Figure 3.3, which we attribute to the differences in van der Waals radii of the halide ions: 1.98 $\mathring{A}$, 1.85 $\mathring{A}$, and 1.75 $\mathring{A}$, for iodine, bromine, and chlorine, respectively.

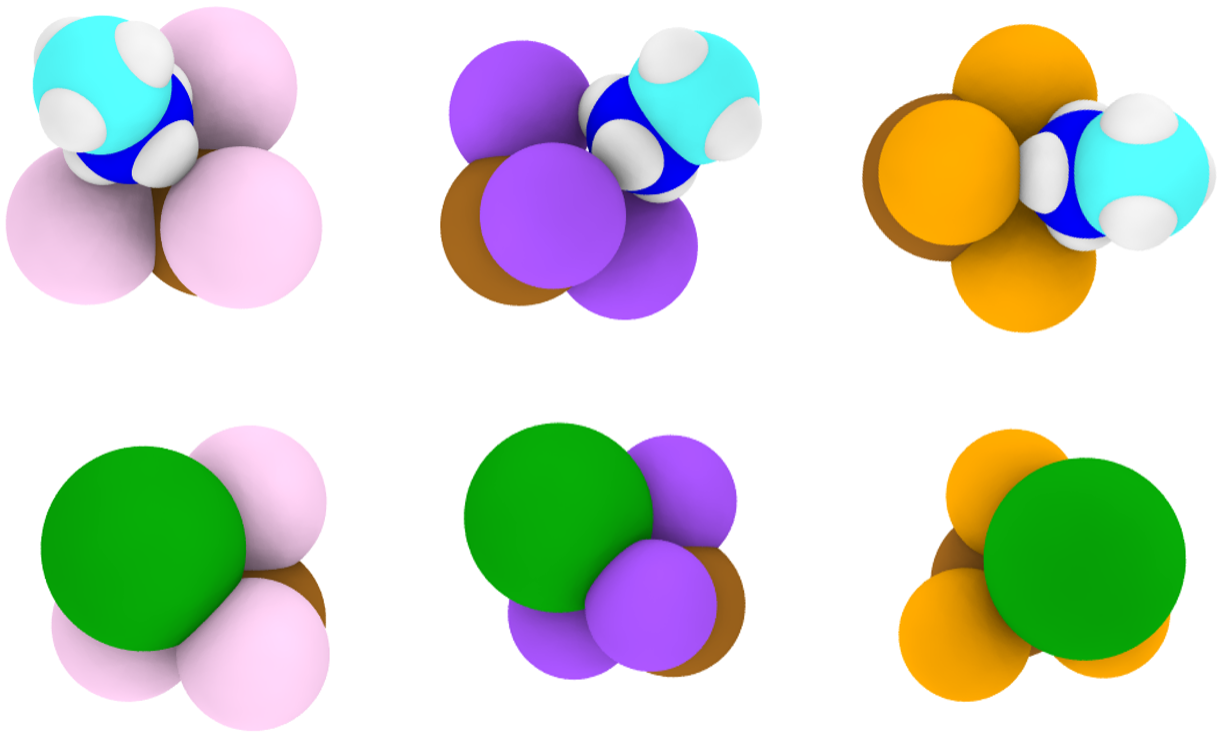

Figure 3.2: Preferred orientations of methylammonium and cesium cation for three choices of halides. In each case, the energy-minimized location of the B-site cation sits in the center of the three halide atoms (whether Cl, Br or I). Color key: pink = iodine, purple = bromine, orange = chlorine, brown = lead, green = cesium, blue = nitrogen, cyan = carbon, white = hydrogen.

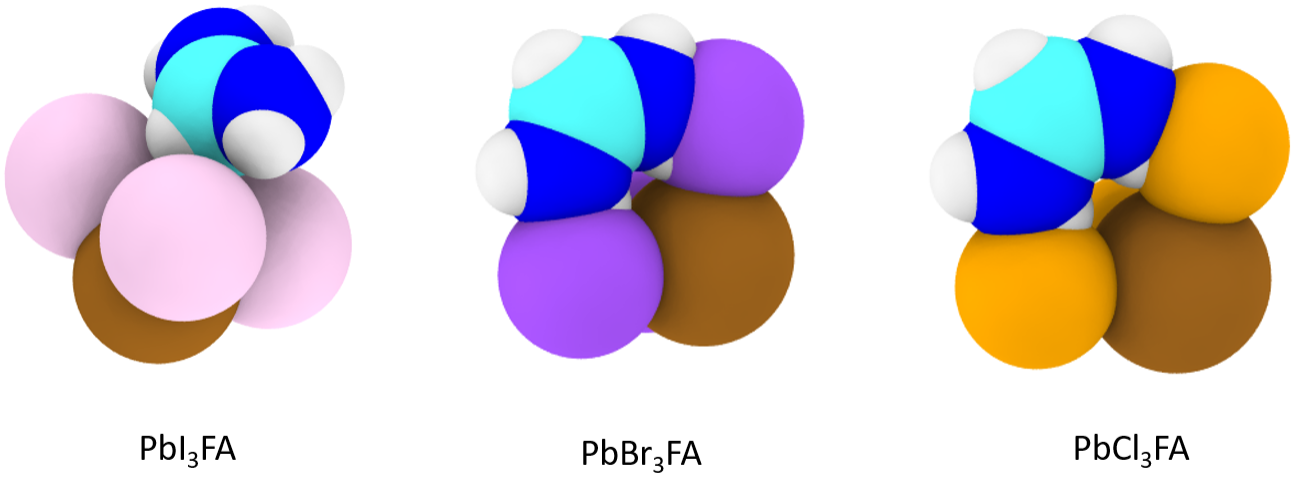

Figure 3.3: Preferred orientations of the formamadinium cation for three choices of halides used in HOIP synthesis. Here, unlike in Fig. 3.2, the larger formamidinium cation bridges two of the halide ions.

3.4 Binding Energy as a function of permittivity

We observed that the relationship between $E_{binding}$ and permittivity was quite predictive for maximizing complexation of the HOIP species in solution. This result implies that the ability of the lead salt and the cation to complex in solution is highly dependent on the permittivity of the solution. The practical advantage of this result is that it provides us with an easy screening metric for other potential anti-solvent candidates that are miscible with the bath solvents.

The relaxed geometries in vacuum, for all the combinations we studied in section 3.3, were further optimized in the presence of an electric field using the permittivity of each pure solvent or anti-solvent in the simulation. Note that the description of the permittivity in these systems does not include explicitly rendered solvent molecules; so no additional atoms or molecules were added while the energy optimizations were performed. Instead, the so-called "implicit solvent" model allows you to create the effect of the electric field in a mean-field representation, and to observe the changes in geometry of these monomers by simply supplying the value of the relative dielectric constant of each choice of solvent or anti-solvent. A list of all bath solvents and anti-solvents that were investigated here are given in Table 3.4 with their relative dielectric constants.

The binding energy for each monomer in each solvent or anti-solvent was calculated using Equation 3.2. Sorting the binding energies in terms of value, it was observed that the lower the permittivity of the solvent, the greater the binding energy of the lead salt to the organic cation. This relationship is true for all the halide and cation combinations we tested. Figure 3.4 shows the trend of binding energy as a function of the inverse relative dielectric (ϵ). Figure 3.4 also shows that the cesium cation exhibits the strongest complexation to the lead salts of all the B-site cations we tested. This is not unexpected as the cesium ion is large, and can form bonds with all three halide atoms on the lead salt. The bond formed between them is also ionic, making the combined network structure stronger and more stable than the hydrogen or covalent bonds that can potentially be formed between the organic cations methylammonium or formamadinium. This is reflected in

the significantly stronger binding energies to cesium. The methylammounium cation also shows a slighter stronger bonding affinity to the lead salts than formamadium, which we can attribute to the number of hydrogen bonds made by each cation. Figures 3.2 and 3.3 show that the amine hydrogens of the methylamonium cation interact with all three halides; whereas, the most stable positions for formamadinum show a weaker contact of hydrogen to halide atoms.

Solvent/Anti-solvent	Dielectric constant
Dimethylsulfoxide	46.7
Tetrahydrothiophene	42.84
gamma-butyrolactone	40.24
Dimethylformamide	36.7
Acetonitrile	35.0
N-Methyl-2-pyrrolidone	32.2
Dimethylacetamide	37.8
Nitromethane	35.87
Nitrobenzene	34.82
Hexamethylphosphoramide	30.0
Acetone	20.7
Trimethylphosphate	20.6
Pyridine	12.4
Methacrolein	10.9
Dichloroethane	10.36
o-dichlorobenzene	9.93
Trifluorotoluene	9.40
Dichloromethane	8.93
Tetrahydrofuran	7.58
Chlorobenzene	5.62
Bromobenzene	5.17
Diethylether	4.33
Anisole	4.33
Toluene	2.38
Benzene	2.27

Table 3.1: List of experimental values for the permittivity (also known as the dielectric constant) for the solvents and anti-solvents studied in this thesis.

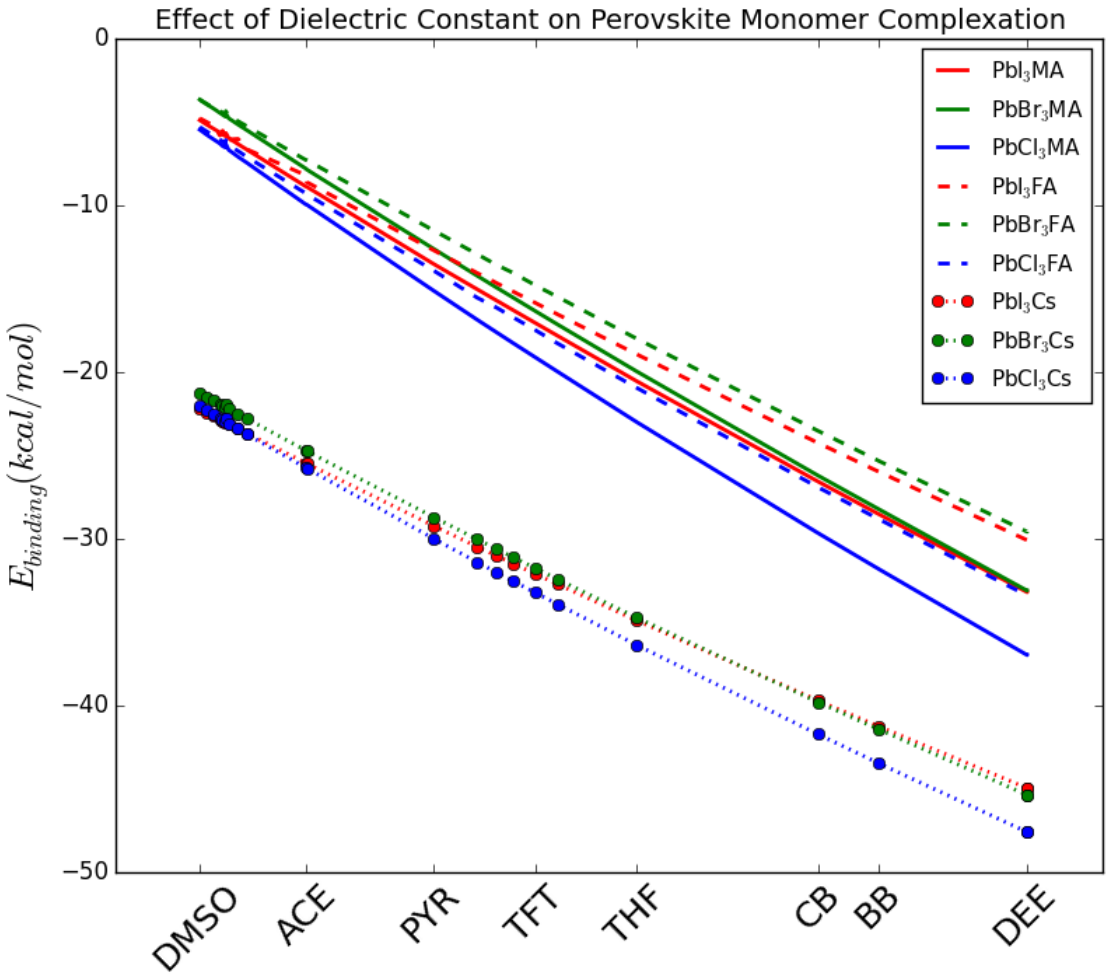

Figure 3.4: Binding energy of PbX_3M as a function of $\frac{1}{\epsilon}$ using an implicit solvent model, showing a roughly linear relationship for a variety of halide and B-site cation choices. Results for the systems containing cesium show a significantly more negative (stronger) binding energy.

As we did in our previous work on complexation, we calculated an electronic property, the Mayer bond order, for each of this new subset of solvents and anti-solvents using a computational protocol as described in Chapter 2. Figure 3.5 shows a three-dimensional plot of the binding energy of PbI_3MA as a function of both the permittivity and the unsaturated Mayer bond order for all the solvents and anti-solvents we studied. A significant difference was identified in the binding energy between PbX_3 and the cation in the presence of anti-solvents compared to the analogous binding energy in bath solvents. The binding energy of PbI_3MA in the experimentally used bath solvent DMSO, was -4.91 kcal/mol, whereas pyridine, an experimentally used anti-solvent, was -13.5 kcal/mol, a far stronger binding. We observed that the unsaturated Mayer bond order does not correlate to the bonding between the lead salts and the cations. This tells us that while the unsaturated Mayer bond order was directly correlated to the enthalpy of solvation (as shown in Chapter 2) and gave us a strong indication of how well that solvent solvated or dissolved the lead salt, it does not provide any indication on the effect of that solvent on the early stages of nucleation of the perovskite building blocks in solution.

Due to the large number of monomer and solvent or anti-solvent combinations that are possible for PbX_3M, a total of 225, we selected a smaller subset to study in detail. Specifically, we chose to look at the PbI_3MA monomer with four solvents or anti-solvents with extremely different relative dielectric constants. We chose dimethylsulfoxide, acetonitrile, trifluorotoluene, and toluene, where ϵ = 46.7, 35.0, 9.40, and 2.38, respectively. We used the results of these selected simulations to compare against the PbI_3MA monomer in vacuum, where $\epsilon = 1$. While these quantities cannot be determined experimentally in a thin film, we used this information as a platform to further study the effect of the solvents and anti-solvents on the bonding between the lead salt and the cation. We determined the electron density using the Mayer bond order, the molecular orbital overlap, the distances between lead and halide atoms, and the halide and amine hydrogens of the methylammonium cation. Table 3.2 shows the variations of these distances for the selected solvents. Whether this difference for the binding of the B-site cation to iodine in dimethylsulfoxide, acetonitrile, trifluorotoluene, and toluene is significant, or not, will have to await our results for

other combinations of halides, B-site cations, and the many other choices of solvents that have been used experimentally.

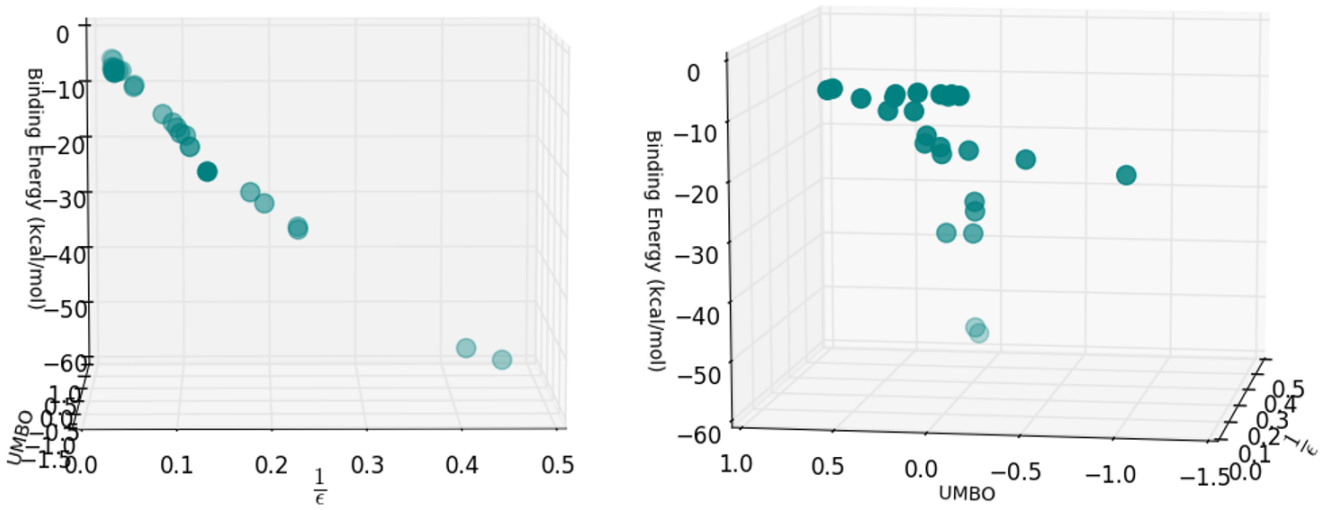

Figure 3.5: Three-dimensional plot of the binding energy of PbI_3MA as a function of $\frac{1}{\epsilon}$, and the unstaurated Mayer bond order of all solvents and anti-solvents used in these computational experiments. The intensity of the color for the graph on the right symbolizes an increase in $\frac{1}{\epsilon}$, with the lightest shade corresponding to 0.5. In the graph on the left, the lighter green indicates a larger, more positive UMBO.

Solvent	Relative Permittivity	Bond	MBO	Distance ($\mathring{A}$)
DMSO	46.7	Pb-I	0.618	3.04
			0.620	3.03
			0.620	3.03
		H-I	-	2.88
			-	2.93
			-	2.90
ACN	35.0	Pb-I	0.620	3.03
			0.622	3.03
			0.622	3.03
		H-I	-	2.87
			-	2.93
			-	2.89
TFT	9.40	Pb-I	0.644	3.02
			0.647	3.02
			0.647	3.02
		H-I	-	2.80
			-	2.84
			-	2.82
TOL	2.38	Pb-I	0.700	2.99
			0.702	2.99
			0.704	2.99
		H-I	0.108	2.70
			0.121	2.66
			0.112	2.68
VAC	1.0	Pb-I	0.737	2.97
			0.740	2.97
			0.740	2.97
		H-I	0.180	2.56
			0.167	2.59
			0.168	2.58

Table 3.2: Variation in MBO and distances between lead, iodine, and hydrogen atoms in the PbI_3MA monomer in four solvents (dimethylsulfoxide (DMSO), acetonitrile, triflourotoluene, toluene) and vacuum.

We observed that, as the relative permittivity decreases, the distance between both the lead and iodine, as well as the distance between the iodine and the amine hydrogens also decreased. While these differences in the distance between pairs of atoms is very small (only 0.07 $\AA$ from DMSO to vacuum), it does support the result that lowering the permittivity of the solution causes the cation and lead salts to be closer to each other, allowing for stronger and shorter bonds to be formed between them. In turn, this has a large effect on the binding energy between the two species. The measured distances between the lead and the halide atoms is approximately 3 $\AA$, and remains essentially the same as the permittivity is varied. The change in distance between the cation's amine hydrogens and the halide atoms on the salt is somewhat more pronounced, with the largest change occurring from DMSO to toluene of a 0.3 $\AA$ difference in distance. This is reasonable, as we know that the more polar bath solvents typically have larger relative dielectric constants, and form stronger dative bonds with the lead, pulling the Pb atom closer to the solvent molecule.

It was surprising to see that a Mayer bond order between the halide and the amine hydrogen was not detectable for any solvent or anti-solvent until the permittivity reached a low value of 2.38, representative of toluene. In our simulations, the Mayer bond order has a cut off of 0.1; anything below this value is not reported as it implies the electron density between two atoms is so small that a bond is not formed between them. Further, if we compare this to a PbI_3MA monomer in vacuum, we see that the MBO between the atoms increases as the relative dielectric decreases. This further implies that lowering the permittivity of the solvent increases the electron density between the cation and the lead salt in solution and therefore will increase the binding energy between the species. To visualize the difference in electron density that exists between the cation and lead salt, we constructed molecular orbital diagrams from the optimized PbI_3MA monomers, as seen in Figure 3.6. It is clear from the these diagrams that the bonding orbital (red) diminishes with increasing relative dielectric.

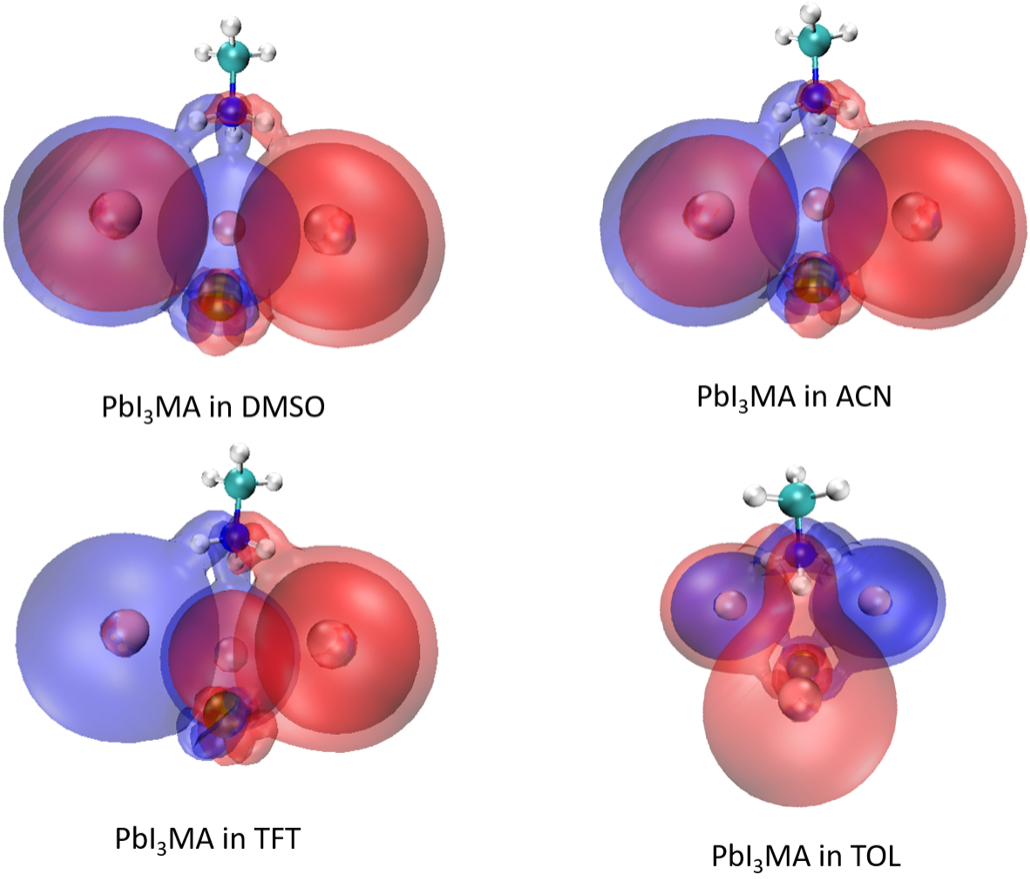

Figure 3.6: Molecular orbital diagrams of PbI_3MA in DMSO, ACN, TFT and TOL. The red in these figures indicates the bonding orbitals, and blue the anti-bonding orbitals.

3.5 An Alternative Approach to Solution Processing

It is known that most bath solvents that dissolve Pb^{2+} will also dissolve the perovskite unit cell, for example, DMSO. But this problem does not look unsolvable. It seems likely that there are solvents and/or solvent blends which have a propensity for dissolving/solubilizing the lead halide, PbX_2, while remaining capable of forming a PbX_3/cation adduct. Using MBO as the metric (as discussed in Chapter 2), we predicted a poor enthalpy of solvation for ACN at -374 kcal/mol, compared to the value for DMSO of -412 kcal/mol. ACN is a low boiling point, highly polar, aprotic solvent which is very often employed in non-aqueous ink formulations. And, as such, ACN is a prime candidate for the solvation of the perovskite precursor salts. However, PbI_2 is completely insoluble in ACN, precluding its use as a solvent for perovskite materials, and further strengthening our MBO work through experimental validation.

Recently, Noel *et al.* [97] investigated using an ACN/MA blend. Their paper noted that while methylammonium iodide, CH_3NH_3I, can be dissolved in neat ACN, PbI_2 can not. The Noel study uses methylamine to enhance the solvating power of acetonitrile, while enabling rapid, room temperature crystallization of methylammonium lead triiodide perovskite films of highly specular quality. Methylamine has a dielectric constant of 9.40, the same as trifluorotoluene (TFT), and very close to tetrahydrofuran (THF), an anti-solvent that we predicted based on its value of the relative dielectric constant. Their experimental work supports our idea that the addition of an anti-solvent that is miscible with the bath solvent and possesses a low relative dielectric can maximize both competing metrics, the solubilization of the lead salts, and optimizing the binding energy between Pbx_3 and the B-site cation.

The use of anti-solvents, is not limited to the common 'anti-solvent drip treatment' during spin casting. The use of anti-solvent baths has been used to fabricate smooth, dense perovskite films with efficiencies of 15% [68]. Zhou *et al.,* dissolved lead salt in NMP and then vertically submerged the perovskite and substrate post-spin-coating into a bath of diethyl ether (DEE) [98]

one of the most commonly used anti-solvent to date [82]. The use of the anti-solvent bath was proposed to induce the growth of perovskite crystals through a 'solvent-anti-solvent' extraction, where the solvent (NMP) diffuses into the anti-solvent (DEE).

In 2015, Shi *et al.,* used a similar method, anti-solvent vapor-assisted crystallization (AVC), where gaseous dichloromethane (DCM) was introduced to a perovskite solution of PbX_2, MAX and DMF, where X= iodine or bromine [99]. This methodology was successful in synthesizing single crystals on the order of millimeters. The results of this study show that growing large, single crystals for HOIPs is possible, but does not provide any support on mechanism or a metric that drives the crystallization in solution. More importantly, this study reoprts no evidence in controlling the crystallization and growth process. The bottleneck with growing large single crystals in solution for HOIPs is further processing them into a thin film. DCM is a liquid at room temperature, and the AVC method requires that DCM be in the gaseous state, requiring temperatures a minimum temperature of 39.6°.

While Chapter Two showed that, at the molecular level, the ability of a solvent or additive to solubilize PbX_2 is well captured by the UMBO, our studies in Chapter Three have uncovered that complexation of the building blocks depends on the relative dielectric properties of the solvent modeled as a mean field-like, "implicit" solvent model. Since we know from experimental studies [8, 82, 84–86] that solvents with a low dielectric constant are effective as an anti-solvent, our studies here suggest that, given the range of dielectric properties available in experimentally used anti-solvents, it should be possible to find one with a higher relative dielectric constant which may help to slightly dissolve or break up perovskite complexes just enough to allow them to rearrange appropriately in solution. Basically, this flexibility in promoting (*via* stronger binding energies) the nucleation of appropriate motifs will provide smaller, sub-critical sized crystallites the mobility in solution to form complexes, rearrange in structure and hence grow into larger nuclei and finally grains.

More speculatively, dissolving perovskite complexes might be undesirable when using bath

solvents, which means bath solvents should have as low a dielectric constant as possible. If this is true, this would allow the design of perovskite solvents on two axes at once, *i.e.,* maximize the solvent's or additive's UMBO value while minimizing its dielectric properties, which can be done by modulation of the permittivity of the solution, typically by the addition of miscible anti-solvents, *prior* to spin-coating. Of course, promoting this viewpoint should await the results of our planned studies of explicit solvent models in comparison to results from to the implicit solvent models used in this Chapter.

In this chapter, we have demonstrated how the permittivity of a solvent can alter the complexation of the pervoskite building blocks. Specifically, our *ab initio* calculations using an implicit solvent model showed that the binding energy between the two major building blocks that go to make up the final perovskite crystal structure can be increased using a relatively low dielectric solvent. It seems logical that if the goal of solution processing is, first, to dissolve the lead salts, and second, to allow nucleation to occur in solution, the addition of a miscible anti-solvent with a lower relative dielectric to a bath solvent with a high UMBO could possibly achieve this. More importantly, we suspect we can optimize these two independent events that occur simultaneously in solution by optimizing the two individual competing metrics for each event over the course of solution processing. First, maximizing the UMBO to dissolve the lead salt, and second, by controlling the addition of an anti-solvent to the bath/anti-solvent solution, we can tune the permittivity of the solution to maximize complexation of perovskite building blocks.

This work has raised the, as yet, experimentally untested hypothesis that the use of low relative dielectric solvents could be employed to provide a degree of control over the nucleation and subsequent growth of perovskite crystals in solution. The systematic methodology demonstrated in this work will enable more efficient and robust selection of the species used in perovskite solution processing, which would then lead to a more precise degree of control over HOIP thin film formation. Ultimately, these molecular-level insights will contribute to accelerating the progress in HOIP solar cell efficiency, scale-up of device manufacturing, better stability and reliability.

3.6 Conclusions

The solution processing of perovskite solar cells is a complex melange involving multiple chemical species and several processing condition vectors and, even with optimal choices of species and conditions, requires an orchestration of the multiple processes that can happen simultaneously if we are to control the outcome in terms of crystalline growth fidelity and large grain sizes. In the solution, there are two key events: the lead salt must be dissolved, and nucleation of the lead halide perovskite structure must then be facilitated to occur.

The results in this thesis have begun to shed light on the effect of solvent choice on these two events. Our work shows that the Mayer bond order is a strong metric for capturing a solvent or additive's ability to dissolve lead salts, an imperative first step in the synthesis of HOIPs. This finding will help quickly evaluate the potential efficacy of any posited solvent or additive. Additionally, we have shown that complexation between the lead salt and the B-site cation increases with decreasing permittivity of the choice of implicitly modeled solvent. We suggest that these two concurrent events can be controlled to maximize the objectives of each over the course of the solution processing cycle. Understanding the driving forces that optimize each event is the key to achieving a high nucleation density and large-grain crystal growth. Our work alludes to the idea that, upon dissolving the lead salt and by subsequent modulation of the relative dielectric characteristics of the solution, we can optimize both of these chemical processes. Crafting a blend that ultimately maximizes the UMBO of the complexes while minimizing the relative dielectric properties could potentially be more effective than the current practice.

Our work here begins to address and understand many puzzle pieces involved in the solvent engineering necessary to create HOIP solar cells. We have shown that the structures we calculated for the Pb^{2+}/solvent complexes tend to be eight-coordinated, not six-coordinated as previously predicted in the literature [30]. No clear pattern of solute geometry is evident in the optimized, sampled complexes, which is consistent with loosely bound, eight-coordinated Pb structures [41].

Prior to this work, the only theory of the effectiveness of HOIP bath solvents available in the literature was that they would be sorted by their empirical relative polarities [49] or Hansen solubility parameters [81]. In this work, we have provided clear evidence that the high bonding power and Lewis basicity, measured by the Mayer bond order, proved more important than any other posited empirical or theoretical properties such as the relative polarity, Hansen polar parameter, molecular dipole moment, atomic charges, or dielectric constant as a metric of determining the solubility of lead salts.

Our calculations confirm the experimental observation that the most powerful current solvent for the perovskite synthesis is DMSO, followed by DMF. Using the Mayer bond order as a screening tool for other, as yet untried, solvents, our calculations suggested that nitromethane and THTO have unusually high (promising) Mayer bond values, but only THTO has a promising bond *unsaturation* value (or UMBO). THTO was shown by the Choi group to fulfill this promise [61]. The presence of two adjacent oxygen atoms in nitromethane showed the importance of considering the Mayer bond *unsaturation* value, rather than the bond order itself. Acetone is also surprisingly effective; in the absence of a methylammonium halide solubility enhancer, it is apparently as effective as GBL. Since acetone is a staple in chemical laboratories, it may be a valuable addition to the HOIP synthesis tool kit, especially with the methylammonium salt and/or in mixtures with other solvents such as DMSO. Use of anti-solvents alludes to another potential benefit: It offers additional control in the complexation and pre-nucleation process, allowing a wider variety of desired and colloidal and solid-state complexation behaviors.

The experimentally observed effect of methylammonium halide as a solubility enhancer is addressed by our cluster geometry calculations, which show that the methylammonium ion stabilizes halide solutes. The $NH_3{}^-$ group can form up to three hydrogen bonds with halide ions, allowing it to stabilize clusters such as PbX_2 and PbX_3. The effect weakens with increasing atomic number of the halide, with $PbI_3{}^+$ having little interaction with $NH_3{}^-$, reflecting the fact that iodide is less capable of hydrogen-bonding than the other halides. Therefore, we cannot yet claim that this effect

fully explains the enhanced solubility caused by methylammonium halides, at least for the iodide salts. What we have observed is the effect of the binding energy between the lead salts and the cation.

In addition, the choice of solvent or anti-solvent plays a crucial role in the degree of complexation between the PbX_3 and B-site cation molecules to form the smallest perovskite building block in solution. As we have shown, the binding energy decreases along with increasing relative dielectric, indicating that the bond strength most likely wanes as well. Our work provides significant evidence that the formation of the monomers strongly correlates to the choice of solvent, specifically the relative dielectric. Given the experimental results from Paek *et al.* [82], we suggest that it is reasonable to expand the search for a solvent/antisolvent combination even further, concentrating on a range of dielectrics between PYR (12.4) and DMF (36.7). What makes this interesting is that the relative dielectric constant of a mixture is a non-linear function of the relative dielectric constants of the components. Thus, when an experimentalist adds an anti-solvent to the bath solvent, the resulting relative dielectric constant will be quite sensitive to the concentration. In theory, the relative dielectric constant of the mixture could be adjusted over the course of the crystallization, modulating the bonding energy of the perovskite complexes to gradually edge the crystallization process to completion in a controlled manner. The appeal to this methodology is that one can potentially grow single crystals directly from solution.

As the ability to control HOIP synthesis grows in importance, control over solution processing aspects will only become more vital. Together with temperature and halide salt composition, solvent choice is one of the few "levers" available with which to continue to improve the efficiency and stability of HOIP solar cells. The theoretical underpinnings we describe, and the fast computational screening techniques we demonstrate, will aid in this process and point the way to more rational solvent engineering for perovskite precursors in the future.

CHAPTER 4

FUTURE WORK

Our studies clearly show the effect of bath solvents and anti-solvents on the complexation between lead salts and B-site cations in the solution processing of perovskite solar cells. It also shows the importance of the choice of solvent in order to achieve the desired nucleation between these species. However, there are issues that still need to be addressed.

Our simulations only take into account the relative dielectric properties of each solvent. The Universal Solvation Model Based on Solute Electron Density (SMD) model in our *ab initio* calculations, used an *implicit* solvent, the quantum mechanical charge density of a solute molecule interacting with a continuum description of the solvent. No simulations were undertaken in which the solvent molecules were *explicitly* modeled while the energetic optimizations were being performed in this work. However, this is an investigation we are currently pursuing. These simulations will be used to determine the error in the implicit SMD model we used. There is quite a lot at stake in this comparison. If we can show even that the trends in solvation produced by the extremely computationally expensive explicit solvent renderings of the system can be adequately reproduced by the faster, cheaper implicit models, this result will be an important result that will allow the community to explore the solution processing landscape more deeply than would be possible using explicit all-atom models.

To expand on our current work, bond dissociation energy calculations could be undertaken for the implicit monomer systems. This would be useful to undertake, as it would provide information on the bond strength between the PbX_3 and B-site cation molecules. This information would also show how that binding strength is affected by the presence of the solvent used. We are currently working with the Choi group in the Chemical Engineering Department at the University of Virginia, who are providing Nuclear Magnetic Resonance (NMR) data on pure solvents. This data will be used to obtain information on the chemical environment of the lead salt in pure solvents,

and to be compared against the chemical environment of the lead salt and cation in the pure solvent. Having the Choi group's *pure* solvent data will be extremely useful since the community is driven by their interests in solvent blends and, hence, no data currently exist for HOIP formation in pure solvents.

As a first step towards this, we made some preliminary calculations of systems containing an explicit (but solitary) single solvent molecule bound to each monomer. Unfortunately, these simulations were more computationally expensive than a simple Universal Solvation Model based on the Solute Electron Density (SMD) model and still did not capture the complexation process as it occurs in experiment. Hence, explicit solvent molecules will need to involve an extremely large DFT calculation for a full sheath of solvent molecules constituting a solvation shell around the monomer. This task is daunting.

To emulate the NMR experiments by the Choi group, we are currently sampling the monomer in the presence of multiple explicit solvent molecules, rather than implementing a simple electric field presence or single solvent molecule. This would allow us to investigate the effect of steric forces upon complexation of the PbX_3 and B-site cation molecules as well as the nucleation of the perovskite crystal from its building blocks. These computational experiments will also be able to take into account solvent-solvent interactions. This would be more useful to the HOIP community as it would better represent experimental work. We are currently sampling all the monomers we studied here, but in the presence of *explicitly modeled* bath solvents: dimethylsulfoxide, dimethylformamide, N-Methyl-2-pyrrolidone, gamma-butlrolactone, acetone, and methacrolein. These experiments involve the same computational methodology as the enthalpy of solvation calculations, as explained in the lead complexation chapter, but since these calculations involve a significantly larger number of atoms, we will need to reduce the number of solvents that we consider so that it is feasible for us to investigate in terms of computational resources. These simulations will also be used to estimate the error in the implicit solvent model.

In addition, we will begin to look at larger perovskite building blocks, as they complex in solu-

tion. The first result of such a reaction is the formation of a proposed perovskite "dimer," as shown in Figure 4.1. A study of the dimerization enthalpies together with their activation energies, E_a, as a function of the choice of solvents, halides and cations, would allow a prediction of the kinetics of the perovskite synthesis. The availability of a high-quality classical HOIP force field would also be immensely helpful in such a study to improve the sampling of the complex geometries that could be involved. Such a force field is under construction by the Clancy group. A classical force field for HOIP materials would be the only viable option to pursue the reaction further to capture n-mer aggregation and reorganization into a HOIP crystal habit.

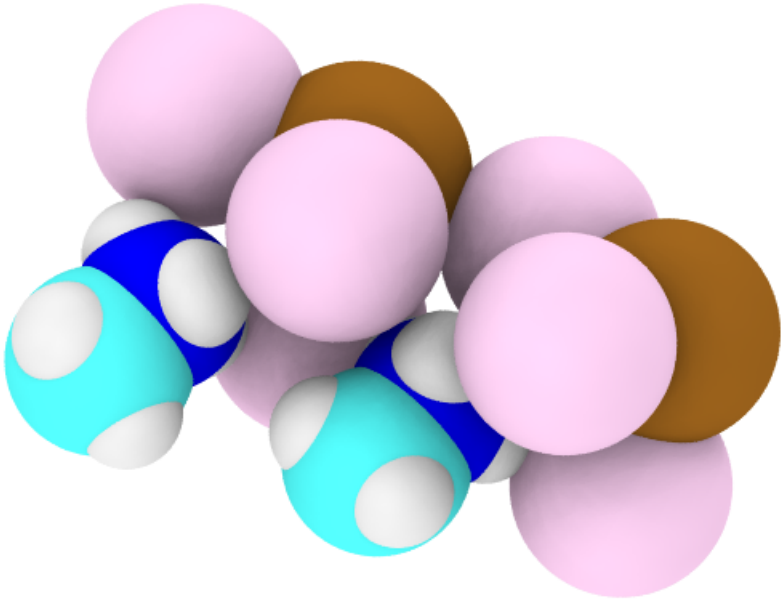

Figure 4.1: A geometry optimized "dimer" complex formed by 2 PbI_3MA monomers. The dimerization occurs by lead-halide bonds formed between the two monomers. The configuration depicts the lowest energy state for a PbI_3MA dimer. The energetically favorable orientation was determined using Nudged Elastic Band (NEB) calculations, as the monomers were rotated from a starting position of 0° to 180°.

Solvent additives, such as a stoichiometric excess of CH_3NH_3I, have also been used to boost the poor solubility of the lead halides (PbX_2) [20]. Figure 2.6 also shows that the more halide ions that are attached to the Pb^{2+} ion, the lower the value of ΔH_{solv}. This is consistent with the idea that the halide ions serve to passivate the Pb^{2+}. The contribution of the halides to the solubility follows the expected periodic trend, with $PbCl_n$ being least soluble and PbI_n being most soluble. In the literature, it has been stated that CH_3NH_3X is a solubility enhancer for PbX_2 simply because CH_3NH_3X adds X^- ions. Their statement draws upon the analogous effect (the so-called "common ion" effect) of adding KI, a source of I^- ions, on PbI_2 solutions [100] (Figure 4.2). The hypothesized mechanism is the formation of PbX_n complexes. However, this explanation is inadequate because the addition of KI to PbI_2 in water does not increase the solubility of PbI_2 above its value in pure water, [101] while the addition of CH_3NH_3X to a solvent does increase the solubility of PbX_2 very significantly [20]. Therefore, the solubility-enhancing effect of CH_3NH_3I must still be regarded as, at least partially, unexplained.

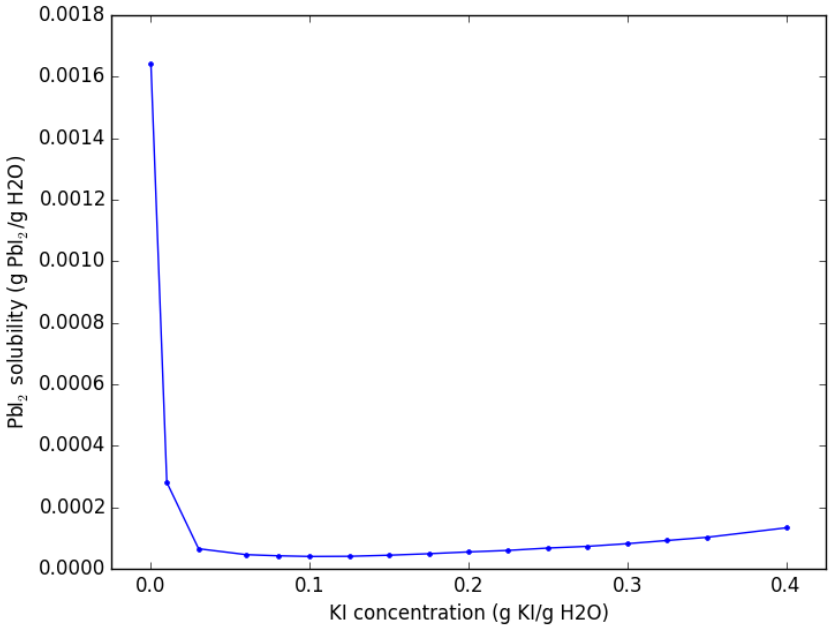

Figure 4.2: The anti-"common-ion" effect, observed for PbI_2 and KI, is shown by the upward slope of the graph with increasing KI concentration. This effect does not fully explain the effect of CH_3NH_3X on PbX_2 solutions in which solubility with CH_3NH_3X is *higher* than the solubility in the pure solvent. Data from Lanford and Kiehl (1941). [101]

BIBLIOGRAPHY

[1] Daryl M Chapin, CS Fuller, and GL Pearson. A new silicon p-n junction photocell for converting solar radiation into electrical power. *Journal of Applied Physics*, 25(5):676–677, 1954.

[2] Hugh L Dryden and AE Von Doenhoff. Solar energy in the exploration of space. *Proceedings of the National Academy of Sciences*, 47(8):1253–1261, 1961.

[3] Jenny Nelson. *The physics of solar cells*. World Scientific Publishing Co Inc, 2003.

[4] Severin Borenstein and James Bushnell. The us electricity industry after 20 years of restructuring. *Annu. Rev. Econ.*, 7(1):437–463, 2015.

[5] Martin Braun, Thomas Stetz, Roland Bründlinger, Christoph Mayr, Kazuhiko Ogimoto, Hiroyuki Hatta, Hiromu Kobayashi, Ben Kroposki, Barry Mather, Michael Coddington, et al. Is the distribution grid ready to accept large-scale photovoltaic deployment? state of the art, progress, and future prospects. *Progress in photovoltaics: Research and applications*, 20 (6):681–697, 2012.

[6] Sarah Kurtz and Greg Wilson. Best research-cell efficiencies may 2016.

[7] Yuanyuan Zhou, Onkar S Game, Shuping Pang, and Nitin P Padture. Microstructures of organometal trihalide perovskites for solar cells: their evolution from solutions and characterization. *The journal of physical chemistry letters*, 6(23):4827–4839, 2015.

[8] Nam Joong Jeon, Jun Hong Noh, Woon Seok Yang, Young Chan Kim, Seungchan Ryu, Jangwon Seo, and Sang Il Seok. Compositional engineering of perovskite materials for high-performance solar cells. *Nature*, 517(7535):476–480, 2015.

[9] Akihiro Kojima, Kenjiro Teshima, Yasuo Shirai, and Tsutomu Miyasaka. Organometal halide perovskites as visible-light sensitizers for photovoltaic cells. *Journal of the American Chemical Society*, 131(17):6050–6051, 2009.

[10] Michael Gratzel. The rise of highly efficient and stable perovskite solar cells. *Accounts of Chemical Research*, 50(3):487–491, 2017.

[11] Michiel L Petrus, Johannes Schlipf, Cheng Li, Tanaji P Gujar, Nadja Giesbrecht, Peter Müller-Buschbaum, Mukundan Thelakkat, Thomas Bein, Sven Hüttner, and Pablo Docampo. Capturing the sun: A review of the challenges and perspectives of perovskite solar cells. *Advanced Energy Materials*, 2017.

[12] Juan-Pablo Correa-Baena, Antonio Abate, Michael Saliba, Wolfgang Tress, T Jesper Jacobsson, Michael Grätzel, and Anders Hagfeldt. The rapid evolution of highly efficient perovskite solar cells. *Energy & Environmental Science*, 10(3):710–727, 2017.

[13] David P McMeekin, Golnaz Sadoughi, Waqaas Rehman, Giles E Eperon, Michael Saliba, Maximilian T Hörantner, Amir Haghighirad, Nobuya Sakai, Lars Korte, Bernd Rech, et al. A mixed-cation lead mixed-halide perovskite absorber for tandem solar cells. *Science*, 351 (6269):151–155, 2016.

[14] Steve Albrecht, Michael Saliba, Juan Pablo Correa Baena, Felix Lang, Lukas Kegelmann, Mathias Mews, Ludmilla Steier, Antonio Abate, Jörg Rappich, Lars Korte, et al. Monolithic perovskite/silicon-heterojunction tandem solar cells processed at low temperature. *Energy & Environmental Science*, 9(1):81–88, 2016.

[15] Xiong Li, Dongqin Bi, Chenyi Yi, Jean-David Décoppet, Jingshan Luo, Shaik Mohammed Zakeeruddin, Anders Hagfeldt, and Michael Grätzel. A vacuum flash–assisted solution process for high-efficiency large-area perovskite solar cells. *Science*, 353(6294):58–62, 2016.

[16] Tadas Malinauskas, Michael Saliba, Taisuke Matsui, Maryte Daskeviciene, Simona Urnikaite, Paul Gratia, Robert Send, Henrike Wonneberger, Ingmar Bruder, Michael Graetzel, et al. Branched methoxydiphenylamine-substituted fluorene derivatives as hole transporting materials for high-performance perovskite solar cells. *Energy & Environmental Science*, 9(5):1681–1686, 2016.

[17] Michael Saliba, Taisuke Matsui, Ji-Youn Seo, Konrad Domanski, Juan-Pablo Correa-Baena, Mohammad Khaja Nazeeruddin, Shaik M Zakeeruddin, Wolfgang Tress, Antonio Abate, Anders Hagfeldt, et al. Cesium-containing triple cation perovskite solar cells: improved stability, reproducibility and high efficiency. *Energy & Environmental Science*, 9(6):1989–1997, 2016.

[18] Jian Gong, Seth B Darling, and Fengqi You. Perovskite photovoltaics: life-cycle assessment of energy and environmental impacts. *Energy & Environmental Science*, 8(7):1953–1968, 2015.

[19] Wanyi Nie, Hsinhan Tsai, Reza Asadpour, Jean-Christophe Blancon, Amanda J Neukirch, Gautam Gupta, Jared J Crochet, Manish Chhowalla, Sergei Tretiak, Muhammad A Alam, et al. High-efficiency solution-processed perovskite solar cells with millimeter-scale grains. *Science*, 347(6221):522–525, 2015.

[20] Keyou Yan, Mingzhu Long, Tiankai Zhang, Zhanhua Wei, Haining Chen, Shihe Yang, and Jianbin Xu. Hybrid halide perovskite solar cell precursors: Colloidal chemistry and coordination engineering behind device processing for high efficiency. *Journal of the American Chemical Society*, 137(13):4460–4468, 2015.

[21] Nam Joong Jeon, Jun Hong Noh, Young Chan Kim, Woon Seok Yang, Seungchan Ryu, and Sang Il Seok. Solvent engineering for high-performance inorganic–organic hybrid perovskite solar cells. *Nat. Mater.*, 13(9):897–903, 2014.

[22] Xiong Li, Dongqin Bi, Chenyi Yi, J.-D. Decoppet, Jingshan Luo, Shaik Mohammed Zakeeruddin, Anders Hagfeldt, and M. Gratzel. A vacuum flash-assisted solution process for high-efficiency large-area perovskite solar cells. *Science*, 8060 (June):1–10, 2016. ISSN 0036-8075. doi: 10.1126/science.aaf8060. URL `http://www.sciencemag.org/cgi/doi/10.1126/science.aaf8060`.

[23] Chang Liu, Kai Wang, Chao Yi, Xiaojun Shi, Adam W Smith, Xiong Gong, and Alan J

Heeger. Efficient perovskite hybrid photovoltaics via alcohol-vapor annealing treatment. *Adv. Funct. Mater.*, 26(1):101–110, 2016.

[24] B Selin Tosun and Hugh W Hillhouse. Enhanced carrier lifetimes of pure iodide hybrid perovskite via vapor-equilibrated re-growth (verg). *J. Phys. Chem. Lett.*, 6(13):2503–2508, 2015.

[25] Ting Zhao, Spencer T Williams, Chu-Chen Chueh, Po-Wei Liang, David S Ginger, and Alex K-Y Jen. Design rules for the broad application of fast (¡ 1 s) methylamine vapor based, hybrid perovskite post deposition treatments. *RSC Adv.*, 6(33):27475–27484, 2016.

[26] Machteld E Kamminga, Hong-Hua Fang, Marina R Filip, Feliciano Giustino, Jacob Baas, Graeme R Blake, Maria Antonietta Loi, and Thomas TM Palstra. Confinement effects in low-dimensional lead iodide perovskite hybrids. *Chemistry of Materials*, 28(13):4554–4562, 2016.

[27] Yuping He and Giulia Galli. Instability and efficiency of mixed halide perovskites ch3nh3ai3–x cl x (a= pb and sn): A first-principles, computational study. *Chemistry of Materials*, 29(2):682–689, 2016.

[28] Claudio Quarti, Edoardo Mosconi, James M Ball, Valerio D'Innocenzo, Chen Tao, Sandeep Pathak, Henry J Snaith, Annamaria Petrozza, and Filippo De Angelis. Structural and optical properties of methylammonium lead iodide across the tetragonal to cubic phase transition: implications for perovskite solar cells. *Energy & Environmental Science*, 9(1):155–163, 2016.

[29] Jarvist M Frost and Aron Walsh. What is moving in hybrid halide perovskite solar cells? *Accounts of chemical research*, 49(3):528–535, 2016.

[30] Seogjoon Yoon, Kevin G Stamplecoskie, and Prashant V Kamat. How lead halide complex chemistry dictates the composition of mixed halide perovskites. *J. Phys. Chem. Lett.*, pages 1368–1373, 2016.

[31] Peter J Holliman, Eurig W Jones, Arthur Connell, Sanjay Ghosh, Leo Furnell, and Robert J Hobbs. Solvent issues during processing and device lifetime for perovskite solar cells. *Mater. Res. Innovations*, 19(7):508–511, 2015.

[32] Xiong Li, M Ibrahim Dar, Chenyi Yi, Jingshan Luo, Manuel Tschumi, Shaik M Zakeeruddin, Mohammad Khaja Nazeeruddin, Hongwei Han, and Michael Grätzel. Improved performance and stability of perovskite solar cells by crystal crosslinking with alkylphosphonic acid ω-ammonium chlorides. *Nat. Chem.*, 2015.

[33] Joseph S Manser, Makhsud I Saidaminov, Jeffrey A Christians, Osman M Bakr, and Prashant V Kamat. Making and breaking of lead halide perovskites. *Accounts of chemical research*, 49(2):330–338, 2016.

[34] Namyoung Ahn, Dae-Yong Son, In-Hyuk Jang, Seong Min Kang, Mansoo Choi, and Nam-Gyu Park. Highly reproducible perovskite solar cells with average efficiency of 18.3% and best efficiency of 19.7% fabricated via lewis base adduct of lead (ii) iodide. *Journal of the American Chemical Society*, 137(27):8696–8699, 2015.

[35] Christian Reichardt and Thomas Welton. *Solvents and solvent effects in organic chemistry*. John Wiley & Sons, 2011.

[36] Adam J Bridgeman, Germán Cavigliasso, Luke R Ireland, and Joanne Rothery. The mayer bond order as a tool in inorganic chemistry. *Journal of the Chemical Society, Dalton Transactions*, (14):2095–2108, 2001.

[37] Adam J Bridgeman and Germán Cavigliasso. Towards an understanding of the bonding in polyoxometalates through bond order and bond energy analysis. *Faraday discussions*, 124: 239–258, 2003.

[38] Robert S Mulliken. Bonding power of electrons and theory of valence. *Chemical Reviews*, 9(3):347–388, 1931.

[39] Seog Joon Yoon, Kevin G Stamplecoskie, and Prashant V Kamat. How lead halide complex chemistry dictates the composition of mixed halide perovskites. *The journal of physical chemistry letters*, 7(7):1368–1373, 2016.

[40] Wei Zhang, Michael Saliba, David T Moore, Sandeep K Pathak, Maximilian T Hörantner, Thomas Stergiopoulos, Samuel D Stranks, Giles E Eperon, Jack A Alexander-Webber, Antonio Abate, et al. Ultrasmooth organic–inorganic perovskite thin-film formation and crystallization for efficient planar heterojunction solar cells. *Nature communications*, 6, 2015.

[41] Ruven L Davidovich, Vitalie Stavila, Dmitry V Marinin, Elena I Voit, and Kenton H Whitmire. Stereochemistry of lead (ii) complexes with oxygen donor ligands. *Coord. Chem. Rev.*, 253(9):1316–1352, 2009.

[42] Lars Goerigk and Stefan Grimme. A thorough benchmark of density functional methods for general main group thermochemistry, kinetics, and noncovalent interactions. *Phys. Chem. Chem. Phys.*, 13(14):6670–6688, 2011.

[43] George A Kaminski, Richard A Friesner, Julian Tirado-Rives, and William L Jorgensen. Evaluation and reparametrization of the OPLS-AA force field for proteins via comparison with accurate quantum chemical calculations on peptides. *The Journal of Physical Chemistry B*, 105(28):6474–6487, 2001.

[44] Stefan Grimme, Jens Antony, Stephan Ehrlich, and Helge Krieg. A consistent and accurate ab initio parametrization of density functional dispersion correction (dft-d) for the 94 elements h-pu. *J. Chem. Phys.*, 132(15):154104, 2010.

[45] Florian Weigend. Accurate coulomb-fitting basis sets for h to rn. *Phys. Chem. Chem. Phys.*, 8(9):1057–1065, 2006.

[46] Shuqiang Niu and Michael B Hall. Theoretical studies on reactions of transition-metal complexes. *Chem. Rev.*, 100(2):353–406, 2000.

[47] Pedro Salvador, Béla Paizs, Miquel Duran, and Sándor Suhai. On the effect of the bsse on intermolecular potential energy surfaces. comparison of a priori and a posteriori bsse correction schemes. *J. Comput. Chem.*, 22(7):765–786, 2001.

[48] James Stevenson, Blaire Sorenson, Varun Hari Subramaniam, James Raiford, Petr P Khlyabich, Yueh-Lin Loo, and Paulette Clancy. Mayer bond order as a metric of complexation effectiveness in lead halide perovskite solutions. *Chemistry of Materials*, 29(6): 2435–2444, 2016.

[49] Namyoung Ahn, Dae-Yong Son, In-Hyuk Jang, Seong Min Kang, Mansoo Choi, and Nam-Gyu Park. Highly reproducible perovskite solar cells with average efficiency of 18.3% and best efficiency of 19.7% fabricated via lewis base adduct of lead (ii) iodide. *J. Am. Chem. Soc.*, 137(27):8696–8699, 2015.

[50] Christian Reichardt. Solvents and solvent effects in organic chemistry, third edition. page 418, 2003.

[51] Charles M Hansen. *Hansen solubility parameters: a user's handbook*. CRC press, 2007.

[52] Steven Abbott and Charles M Hansen. *Hansen solubility parameters in practice*. Hansen-Solubility, 2008.

[53] Derek YC Chan, D John Mitchell, and Barry W Ninham. A model of solvent structure around ions. *J. Chem. Phys.*, 70(6):2946–2957, 1979.

[54] Ingmar Persson, Krzysztof Lyczko, Daniel Lundberg, Lars Eriksson, and Anna Płaczek. Coordination chemistry study of hydrated and solvated lead (ii) ions in solution and solid state. *Inorganic chemistry*, 50(3):1058–1072, 2011.

[55] Woon Seok Yang, Jun Hong Noh, Nam Joong Jeon, Young Chan Kim, Seungchan Ryu, Jangwon Seo, and Sang Il Seok. High-performance photovoltaic perovskite layers fabricated through intramolecular exchange. *Science*, 348(6240):1234–1237, 2015.

[56] Wenzhe Li, Jiandong Fan, Jiangwei Li, Yaohua Mai, and Liduo Wang. Controllable grain morphology of perovskite absorber film by molecular self-assembly toward efficient solar cell exceeding 17%. *Journal of the American Chemical Society*, 137(32):10399–10405, 2015.

[57] Yaoguang Rong, Zhongjia Tang, Yufeng Zhao, Xin Zhong, Swaminathan Venkatesan, Harrison Graham, Matthew Patton, Yan Jing, Arnold M Guloy, and Yan Yao. Solvent engineering towards controlled grain growth in perovskite planar heterojunction solar cells. *Nanoscale*, 7(24):10595–10599, 2015.

[58] Jin Hyuck Heo, Dae Ho Song, Hye Ji Han, Seong Yeon Kim, Jun Ho Kim, Dasom Kim, Hee Won Shin, Tae Kyu Ahn, Christoph Wolf, Tae-Woo Lee, et al. Planar ch3nh3pbi3 perovskite solar cells with constant 17.2% average power conversion efficiency irrespective of the scan rate. *Advanced Materials*, 27(22):3424–3430, 2015.

[59] Seunghwan Bae, Seung Jin Han, Tae Joo Shin, and Won Ho Jo. Two different mechanisms of ch3nh3pbi3 film formation in one-step deposition and its effect on photovoltaic properties of opv-type perovskite solar cells. *Journal of Materials Chemistry A*, 3(47):23964–23972, 2015.

[60] Yaoguang Rong, Swaminathan Venkatesan, Rui Guo, Yanan Wang, Jiming Bao, Wenzhi Li, Zhiyong Fan, and Yan Yao. Critical kinetic control of non-stoichiometric intermediate phase transformation for efficient perovskite solar cells. *Nanoscale*, 8(26):12892–12899, 2016.

[61] Benjamin J Foley, Justin Girard, Blaire A Sorenson, Alexander Z Chen, J Scott Niezgoda, Matthew R Alpert, Angela F Harper, Detlef-M Smilgies, Paulette Clancy, and Wissam A Saidi. Controlling nucleation, growth, and orientation of metal halide perovskite thin films with rationally selected additives. *J. Mater. Chem. A*, 2016.

[62] Feng Hao, Constantinos C Stoumpos, Zhao Liu, Robert PH Chang, and Mercouri G Kanatzidis. Controllable perovskite crystallization at a gas–solid interface for hole

conductor-free solar cells with steady power conversion efficiency over 10%. *Journal of the American Chemical Society*, 136(46):16411–16419, 2014.

[63] Fuzhi Huang, Yasmina Dkhissi, Wenchao Huang, Manda Xiao, Iacopo Benesperi, Sergey Rubanov, Ye Zhu, Xiongfeng Lin, Liangcong Jiang, Yecheng Zhou, et al. Gas-assisted preparation of lead iodide perovskite films consisting of a monolayer of single crystalline grains for high efficiency planar solar cells. *Nano Energy*, 10:10–18, 2014.

[64] Yani Chen, Yixin Zhao, and Ziqi Liang. Non-thermal annealing fabrication of efficient planar perovskite solar cells with inclusion of nh4cl. *Chemistry of Materials*, 27(5):1448–1451, 2015.

[65] Xin Guo, Christopher McCleese, Charles Kolodziej, Anna CS Samia, Yixin Zhao, and Clemens Burda. Identification and characterization of the intermediate phase in hybrid organic–inorganic mapbi 3 perovskite. *Dalton Transactions*, 45(9):3806–3813, 2016.

[66] Hung-Ju Yen, Po-Wei Liang, Chu-Chen Chueh, Zhibin Yang, Alex K-Y Jen, and Hsing-Lin Wang. Large grained perovskite solar cells derived from single-crystal perovskite powders with enhanced ambient stability. *ACS applied materials & interfaces*, 8(23):14513–14520, 2016.

[67] Manda Xiao, Fuzhi Huang, Wenchao Huang, Yasmina Dkhissi, Ye Zhu, Joanne Etheridge, Angus Gray-Weale, Udo Bach, Yi-Bing Cheng, and Leone Spiccia. A fast deposition-crystallization procedure for highly efficient lead iodide perovskite thin-film solar cells. *Angewandte Chemie*, 126(37):10056–10061, 2014.

[68] Yuanyuan Zhou, Mengjin Yang, Wenwen Wu, Alexander L Vasiliev, Kai Zhu, and Nitin P Padture. Room-temperature crystallization of hybrid-perovskite thin films via solvent–solvent extraction for high-performance solar cells. *Journal of Materials Chemistry A*, 3 (15):8178–8184, 2015.

[69] Chun-Chao Chen, Zirou Hong, Gang Li, Qi Chen, Huanping Zhou, and Yang Yang. One-step, low-temperature deposited perovskite solar cell utilizing small molecule additive. *Journal of Photonics for Energy*, 5(1):057405–057405, 2015.

[70] Zhongmin Zhou, Zaiwei Wang, Yuanyuan Zhou, Shuping Pang, Dong Wang, Hongxia Xu, Zhihong Liu, Nitin P Padture, and Guanglei Cui. Methylamine-gas-induced defect-healing behavior of ch3nh3pbi3 thin films for perovskite solar cells. *Angewandte Chemie International Edition*, 54(33):9705–9709, 2015.

[71] Mengjin Yang, Yuanyuan Zhou, Yining Zeng, Chun-Sheng Jiang, Nitin P Padture, and Kai Zhu. Square-centimeter solution-processed planar ch3nh3pbi3 perovskite solar cells with efficiency exceeding 15%. *Advanced Materials*, 27(41):6363–6370, 2015.

[72] David T Moore, Kwan W Tan, Hiroaki Sai, Katherine P Barteau, Ulrich Wiesner, and Lara A Estroff. Direct crystallization route to methylammonium lead iodide perovskite from an ionic liquid. *Chemistry of Materials*, 27(9):3197–3199, 2015.

[73] Kwan Wee Tan, David T Moore, Michael Saliba, Hiroaki Sai, Lara A Estroff, Tobias Hanrath, Henry J Snaith, and Ulrich Wiesner. Thermally induced structural evolution and performance of mesoporous block copolymer-directed alumina perovskite solar cells. *Acs Nano*, 8(5):4730–4739, 2014.

[74] Huanping Zhou, Qi Chen, Gang Li, Song Luo, Tze-bing Song, Hsin-Sheng Duan, Ziruo Hong, Jingbi You, Yongsheng Liu, and Yang Yang. Interface engineering of highly efficient perovskite solar cells. *Science*, 345(6196):542–546, 2014.

[75] Samuel D Stranks, Giles E Eperon, Giulia Grancini, Christopher Menelaou, Marcelo JP Alcocer, Tomas Leijtens, Laura M Herz, Annamaria Petrozza, and Henry J Snaith. Electron-hole diffusion lengths exceeding 1 micrometer in an organometal trihalide perovskite absorber. *Science*, 342(6156):341–344, 2013.

[76] Qiuju Liang, Jiangang Liu, Zhongkai Cheng, Yan Li, Liang Chen, Rui Zhang, Jidong Zhang, and Yanchun Han. Enhancing the crystallization and optimizing the orientation of perovskite films via controlling nucleation dynamics. *Journal of Materials Chemistry A*, 4(1):223–232, 2016.

[77] Guangda Niu, Hongde Yu, Jiangwei Li, Dong Wang, and Liduo Wang. Controlled orientation of perovskite films through mixed cations toward high performance perovskite solar cells. *Nano Energy*, 27:87–94, 2016.

[78] Michael M Lee, Joël Teuscher, Tsutomu Miyasaka, Takurou N Murakami, and Henry J Snaith. Efficient hybrid solar cells based on meso-superstructured organometal halide perovskites. *Science*, 338(6107):643–647, 2012.

[79] Julian Burschka, Norman Pellet, Soo-Jin Moon, Robin Humphry-Baker, Peng Gao, Mohammad K Nazeeruddin, and Michael Grätzel. Sequential deposition as a route to high-performance perovskite-sensitized solar cells. *Nature*, 499(7458):316–319, 2013.

[80] Mingzhen Liu, Michael B Johnston, and Henry J Snaith. Efficient planar heterojunction perovskite solar cells by vapour deposition. *Nature*, 501(7467):395–398, 2013.

[81] Kira L. Gardner, Jeffrey G. Tait, Tamara Merckx, Weiming Qiu, Ulrich W. Paetzold, Lucinda Kootstra, Manoj Jaysankar, Robert Gehlhaar, David Cheyns, Paul Heremans, and Jef Poortmans. Nonhazardous Solvent Systems for Processing Perovskite Photovoltaics. *Adv. Energy Mater.*, 2016. doi: 10.1002/aenm.201600386. URL `http://doi.wiley.com/10.1002/aenm.201600386`.

[82] S Paek, P Schouwink, E Nefeli Athanasopoulou, KT Cho, G Grancini, Y Lee, Y Zhang, F Stellacci, Mohammad Khaja Nazeeruddin, and P Gao. From nano-to micrometer scale: The role of antisolvent treatment on high performance perovskite solar cells. *Chemistry of Materials*, 29(8):3490–3498, 2017.

[83] Byeong Jo Kim, Dong Hoe Kim, Seung Lee Kwon, So Yeon Park, Zhen Li, Kai Zhu, and Hyun Suk Jung. Selective dissolution of halide perovskites as a step towards recycling solar cells. *Nature communications*, 7, 2016.

[84] Dongqin Bi, Wolfgang Tress, M Ibrahim Dar, Peng Gao, Jingshan Luo, Clémentine Renevier, Kurt Schenk, Antonio Abate, Fabrizio Giordano, Juan-Pablo Correa Baena, et al. Efficient luminescent solar cells based on tailored mixed-cation perovskites. *Science advances*, 2(1):e1501170, 2016.

[85] Dae-Yong Son, Jin-Wook Lee, Yung Ji Choi, In-Hyuk Jang, Seonhee Lee, Pil J Yoo, Hyunjung Shin, Namyoung Ahn, Mansoo Choi, Dongho Kim, et al. Self-formed grain boundary healing layer for highly efficient ch3 nh3 pbi3 perovskite solar cells. *Nature Energy*, 1: 16081, 2016.

[86] Hong Zhang, Jiaqi Cheng, Dan Li, Francis Lin, Jian Mao, Chunjun Liang, Alex K-Y Jen, Michael Grätzel, and Wallace CH Choy. Toward all room-temperature, solution-processed, high-performance planar perovskite solar cells: A new scheme of pyridine-promoted perovskite formation. *Advanced Materials*, 29(13), 2017.

[87] F Neese and F Wennmohs. Orca (v. 3.0. 3). *An ab initio, DFT and semiempirical SCF-MO package, Max-Planck-Institute for Chemical Energy Conversion, Stiftstr*, pages 34–36.

[88] Yan Zhao and Donald G Truhlar. Design of density functionals that are broadly accurate for thermochemistry, thermochemical kinetics, and nonbonded interactions. *The Journal of Physical Chemistry A*, 109(25):5656–5667, 2005.

[89] Florian Weigend and Reinhart Ahlrichs. Balanced basis sets of split valence, triple zeta valence and quadruple zeta valence quality for h to rn: Design and assessment of accuracy. *Physical Chemistry Chemical Physics*, 7(18):3297–3305, 2005.

[90] Stefan Grimme, Jens Antony, Stephan Ehrlich, and Helge Krieg. A consistent and accu-

rate ab initio parametrization of density functional dispersion correction (dft-d) for the 94 elements h-pu. *The Journal of chemical physics*, 132(15):154104, 2010.

[91] Stefan Grimme, Stephan Ehrlich, and Lars Goerigk. Effect of the damping function in dispersion corrected density functional theory. *Journal of computational chemistry*, 32(7): 1456–1465, 2011.

[92] Bernhard Metz, Hermann Stoll, and Michael Dolg. Small-core multiconfiguration-dirac–hartree–fock-adjusted pseudopotentials for post-d main group elements: application to pbh and pbo. *The Journal of Chemical Physics*, 113(7):2563–2569, 2000.

[93] Kirk A Peterson, Detlev Figgen, Erich Goll, Hermann Stoll, and Michael Dolg. Systematically convergent basis sets with relativistic pseudopotentials. ii. small-core pseudopotentials and correlation consistent basis sets for the post-d group 16–18 elements. *The Journal of chemical physics*, 119(21):11113–11123, 2003.

[94] Holger Kruse and Stefan Grimme. A geometrical correction for the inter-and intra-molecular basis set superposition error in hartree-fock and density functional theory calculations for large systems. *The Journal of chemical physics*, 136(15):04B613, 2012.

[95] Aleksandr V Marenich, Christopher J Cramer, and Donald G Truhlar. Universal solvation model based on solute electron density and on a continuum model of the solvent defined by the bulk dielectric constant and atomic surface tensions. *The Journal of Physical Chemistry B*, 113(18):6378–6396, 2009.

[96] Aleksandr V Marenich, Christopher J Cramer, and Donald G Truhlar. Performance of sm6, sm8, and smd on the sampl1 test set for the prediction of small-molecule solvation free energies. *The Journal of Physical Chemistry B*, 113(14):4538–4543, 2009.

[97] Nakita K Noel, Severin N Habisreutinger, Bernard Wenger, Matthew T Klug, Maximilian T Hörantner, Michael B Johnston, Robin J Nicholas, David T Moore, and Henry J Snaith. A

low viscosity, low boiling point, clean solvent system for the rapid crystallisation of highly specular perovskite films. *Energy & Environmental Science*, 10(1):145–152, 2017.

[98] Yuanyuan Zhou, Mengjin Yang, Onkar S Game, Wenwen Wu, Joonsuh Kwun, Martin A Strauss, Yanfa Yan, Jinsong Huang, Kai Zhu, and Nitin P Padture. Manipulating crystallization of organolead mixed-halide thin films in antisolvent baths for wide-bandgap perovskite solar cells. *ACS applied materials & interfaces*, 8(3):2232–2237, 2016.

[99] Dong Shi, Valerio Adinolfi, Riccardo Comin, Mingjian Yuan, Erkki Alarousu, Andrei Buin, Yin Chen, Sjoerd Hoogland, Alexander Rothenberger, Khabiboulakh Katsiev, et al. Low trap-state density and long carrier diffusion in organolead trihalide perovskite single crystals. *Science*, 347(6221):519–522, 2015.

[100] Yongping Fu, Fei Meng, Matthew B Rowley, Blaise J Thompson, Melinda J Shearer, Dewei Ma, Robert J Hamers, John C Wright, and Song Jin. Solution growth of single crystal methylammonium lead halide perovskite nanostructures for optoelectronic and photovoltaic applications. *J. Am. Chem. Soc.*, 137(17):5810–5818, 2015.

[101] Oscar E. Lanford and Samuel J. Kiehl. The solubility of lead iodide in solutions of potassium iodide-complex lead iodide ions. *J. Am. Chem. Soc.*, 63(3):667–669, 1941. doi: 10.1021/ja01848a010.